

DISSERTATIONS IN
**FORESTRY AND
NATURAL SCIENCES**

PESAL KOIRALA

*Simulation and
Measurement of Colored
Surfaces*

PUBLICATIONS OF THE UNIVERSITY OF EASTERN FINLAND
Dissertations in Forestry and Natural Sciences No 102



UNIVERSITY OF
EASTERN FINLAND

PESAL KOIRALA

*Simulation and
Measurement of Colored
Surfaces*

Publications of the University of Eastern Finland
Dissertations in Forestry and Natural Sciences
No 102

Academic Dissertation

To be presented by permission of the Faculty of Science and Forestry
for public examination in the Louhela Auditorium in Science Park, Joensuu,
on April 19, 2013 at 12 o'clock noon.

School of Computing

Kopijyvä Oy

Joensuu, 2013

Editor: Profs. Pertti Pasanen, Pekka Kilpeläinen, Kai Peiponen, and Matti
Vornanen

Distribution:

University of Eastern Finland Library / Sales of publications

P.O. Box 107, FI-80101 Joensuu, Finland

tel. +358-50-3058396

<http://www.uef.fi/kirjasto>

ISBN: 978-952-61-1078-3 (printed)

ISSNL: 1798-5668

ISSN: 1798-5668

ISBN: 978-952-61-1079-0 (pdf)

ISSN: 1798-5676 (pdf)

Author's address: Norsk Elektro Optikk AS
P.O.Box 384
N-1473 Lørenskog
NORWAY
email: pesal@neo.no

Supervisors: Professor Markku Hauta-Kasari, PhD
University of Eastern Finland
School of Computing
P.O.Box 111
FI-80101 Joensuu
FINLAND
email: markku.hauta-kasari@uef.fi

Professor Jussi Parkkinen, PhD
University of Eastern Finland
School of Computing
P.O.Box 111
80101 Joensuu
FINLAND
email: jussi.parkkinen@uef.fi

Current address:
Monash University Sunway Campus
School of Engineering
Jalan Lagoon Selatan, 46150 Bandar Sunway
Selangor Darul Ehsan, Malaysia

Reviewers: Professor Jari Hannuksela, Dr. Tech
University of Oulu
Center for Machine Vision Research
Department of Computer Science and Engineering
P.O Box 4500
FI-90014 Oulu
Finland
email: jhannuks@ee.oulu.fi

Principal Researcher Antonio Robles-Kelly, PhD
NICTA
Canberra Research Laboratory
Tower A, 7 London Circuit
Locked Bag 8001
Canberra ACT 2601
Australia
email: Antonio.Robles-Kelly@nicta.com.au

Opponent: Professor Dietrich Paulus, Dr.-Ing
University of Koblenz-Landau
Universitätsstr. 1
56070 Koblenz
Germany
email: paulus@uni-koblenz.de

ABSTRACT

Spectral imaging is becoming more common for quality inspection processes in industrial applications. Spectral imaging, generally known as hyperspectral imaging, is widely used in remote sensing. The application of spectral imaging is growing in the fields of forestry, agriculture and computer vision. The large number of bands in spectral imaging provides a large set of information offering considerable opportunities in image analysis. The bottleneck in spectral imaging is on the processing side, in the handling of the large sized data sets. Nevertheless, spectral image processing is going to be more popular proportional to the cheap memory and processing speed .

In the thesis, three computational research topics have been chosen in which to employ spectral imaging. In the first case, the spectra of mixed pigments were simulated, and more interestingly the spectra of mixing pigments and their concentrations were predicted. The pigments were coated on round plastic pipes. The core principle behind this was the Kubelka-Munk method. In the second case, spectra in multi-angle measurement were predicted. The best viewing angles were determined to predict correct reflectance. Principal component analysis and the Wiener estimation method were applied on metallic and pearlescent samples to accurately predict reflectance. In the third case, the highlight removal method for RGB and spectral images were proposed. Principal component analysis and histogram equalization were used to obtain a diffuse RGB image from the given highlight-affected RGB image. Similarly, the spectral unmixing method was proposed to obtain a diffuse spectral image from a given highlight-affected spectral image.

Universal Decimal Classification: 004.932, 535.312, 535.33, 535.6

Keywords (INSPEC Thesaurus): imaging; spectra; spectral analysis; image processing; colour; image colour analysis; colorimetry; pigments; angular measurement; reflectivity; principal component analysis.

Keywords (Yleinen suomalainen asiasanasto): spektrikuvaus; spektrianalyysi; värit; pigmentit; heijastuminen.

Preface

First I would like to express my sincere gratitude to Prof. Markku Hauta-Kasari and Prof. Jussi Parkkinen for providing me with the opportunity to conduct a PhD under their supervision. Without their continuous guidance and motivation this PhD would not be finished. I am grateful to all the staff at the Department of Computer Science of the University of Joensuu, since each and every piece of help was indispensable for the successful completion of my degree.

I would like to thank Exel and Ruukki for their industrial cooperation. The research could not have been performed without their active cooperation.

I would like to thank Dr. Jouni Hiltunen for guidance in the lab. I would also like to thank Dr. Birgitta Martinkauppi for providing guidance during my research. I would like to express my gratitude to Dr. Vladimir Bochko for providing the sample data set for the comparative study. I would also like to thank Mrs. Merja Hyttinen for her care and support. I would like to thank Mr. Paras Pant for discussing research matters with me. I would like to express my gratitude to all my colleagues in the color research laboratory, Juha Lehtonen, Jussi Kinnunen, Ville Hautamäki, Jukka Antikainen, Tuija Jetsu, Olli Kohonen, Ville Heikkinen, Pauli Fält, Alexey Andriyashin, Tommi Pakarinen, Masayuki Ukishima and Hongyu Li. They provided me a very friendly working environment. In the meantime, I would like to remember Paras Pant, Muskan Regmi, Surya Magar, Ajaya Mishra, Pratigya Khanal, Eliza Poudel, Basanta Raj Gautam, Yamuna Gautam and Ghanshyam Bishwakarma. Having all these wonderful people in Joensuu I never felt I was far from my home country. I am incredibly grateful to Norsk Elektro Optikk and particularly to Ivar Baarstad for always being positive towards my PhD study.

I would like to thank my siblings for their love and motivation

towards my studies. I would like to thank my wife Shiva for her endless support and love. Finally, without the blessings of my parents, this PhD thesis could not have been finished, I am always indebted to them.

Lørenskog Dec 8, 2012

Pesal Koirala

ABBREVIATIONS

ANC	Abundance non negativity constraint
ANOVA	Analysis of variance
ASC	Abundance sum to one constraint
ASTM	American society for testing and materials
ATGP	Automated target generation program
BRDF	Bidirectional Reflectance Distribution Function
CCD	Charged coupled device
CEM	Constrained energy minimization
CIE	Commission internationale de l'éclairage
DIN	Deutsches institut für normung (German institute for standardization)
DRM	Dichromatic reflection model
FIR	Finite impulse response
GFC	Goodness of fit coefficient
KM	Kubelka-Munk
LCTF	Liquid crystal tunable filter
LLS	Linear least square
MSF	Modified specular free
OSP	Orthogonal subspace projection
PC	Principal component
PCA	Principal component analysis
PCV	Principal component vector
PPCA	Probabilistic principal component analysis
PVDF	Polyvinylidene fluoride
RMS	Root mean square
RMSE	Root mean square error
SAM	Spectral angle mapper
SF	Specular free
SPD	Spectral power distribution
VNIR	Very near infrared region

LIST OF PUBLICATIONS

- 1 P. Koirala, M. Hauta-Kasari, B. Martinkauppi, and J. Hiltunen, "Color Mixing and Color Separation of Pigments with Concentration Prediction," *Color Research and Application*, Volume 33, Issue 6, 461–469, 2008.
- 2 P. Koirala, M. Hauta-Kasari, J. Parkkinen, and J. Hiltunen, "Accurate reflectance prediction in multi-angle measurement," *4th European Conference on Colour in Graphics, Imaging, and Vision (CGIV 2008/MCS'08)*, Terrassa, Spain, 489–493, June 9-13, 2008.
- 3 P. Koirala, M. Hauta-Kasari, J. Parkkinen, and J. Hiltunen, "Reflectance Prediction in Multi-Angle Measurement by Wiener Estimation Method," *16th Color Imaging Conference*, Portland, Oregon, USA, 221–226, November 10-15, 2008.
- 4 P. Koirala, M. Hauta-Kasari, and J. Parkkinen, "Highlight Removal from Single Image," *Advanced Concepts for Intelligent Vision Systems (ACIVS 2009)*, Bordeaux, France, Lecture Notes in Computer Science, Springer LNCS, 176–187, September 28-October 2, 2009
- 5 P. Koirala, P. Pant, M. Hauta-Kasari, and J. Parkkinen "Highlight Detection and Removal from Spectral Image," *Journal of Optical Society of America A*, Volume 28, Number 11, 2284–2291, 2011.

Throughout the thesis these publications will be referred to as *Publication 1*, *Publication 2*, *Publication 3*, *Publication 4*, and *Publication 5*. *Publication 1* and *Publication 5* are peer reviewed scientific journal articles, and *Publication 2* to *Publication 4* are peer reviewed conference articles. The publications have been included at the end of the thesis with permission of their copyright holders.

AUTHOR'S CONTRIBUTION

The publications in this dissertation are original research papers, and the contributions of the author are summarized as follows.

The idea of *Publication 1* originated from collaborations between the author and co-authors regarding solving industrial problems in color mixing and unmixing. The required samples for the training and test sets were measured by the author and co-author, Jouni Hiltunen. All the samples were received from the Exel as a part of industrial cooperation.

The idea of *Publication 2* and *Publication 3* originated from collaborations between the author and co-authors on the prediction of reflectance in multi-angle measurement. The author and co-author, Jouni Hiltunen, produced the setup for the measurement for the training and test sets of samples, and all the measurements were carried out by the author. All the samples were received from Ruukki as a part of industrial cooperation.

The idea of *Publication 4* and *Publication 5* originated from collaborations between the author and co-author, Markku Hauta-Kasari. In *Publication 5* some of the samples were measured by the co-author Paras Pant.

In all publications, the author has carried out all numerical computations, and selected and developed the required algorithms. The author has written all the papers mentioned. The author and all the co-authors collaborated closely when writing the manuscript to paper, according to the reviewers' suggestions. The co-operation with the co-authors has been significant.

Contents

1	INTRODUCTION	1
2	RESEARCH PROBLEMS ADDRESSED IN THIS THESIS	7
3	LIGHT SURFACE INTERACTION	13
3.1	Reflection Measurement	13
3.2	Reflectance Calculation	15
3.3	Dichromatic Reflection Model	16
3.3.1	Formulation of Dichromatic Reflection Model	17
3.3.2	Multiple Illuminations	19
3.4	Decomposition of Reflection	20
4	SPECTRAL COLOR MIXING AND UNMIXING	23
4.1	Previous Works	24
4.2	Sample preparation	25
4.3	Kubelka-Munk Method	26
4.4	Reflection correction	29
4.5	Spectral color mixing	31
4.6	Spectral color unmixing	35
4.6.1	Concentration Prediction	36
4.6.2	Pigment Selection	37
4.7	Discussion	39
5	MULTI-ANGLE MEASUREMENT	43
5.1	Previous Works	44
5.2	Sample Preparation	45
5.3	Measurement Angles	48
5.4	Principal Component Analysis	49
5.4.1	Prediction by PCA	50
5.5	Wiener estimation	52
5.6	Discussion	54

6	HIGHLIGHT REMOVAL FROM SINGLE IMAGE	59
6.1	Previous Works	60
6.2	Highlight detection	61
6.2.1	Highlight detection in difference image	62
6.2.2	Highlight detection by CEM	63
6.3	Diffuse image from RGB image	64
6.4	Diffuse image from spectral image	65
6.5	Quality measure of diffuse image	67
6.6	Discussion	68
7	DISCUSSION	73
	BIBLIOGRAPHY	76
A	APPENDIX: SUPPORTING EQUATIONS	87
A.1	Kubelka-Munk Method Formulation	87
A.2	Color difference	89
A.2.1	CIELAB color difference	90
A.2.2	S-CIELAB color difference	90
A.2.3	CMC (l:c) color difference	92
A.3	Spectral difference	94
A.3.1	Root Mean Square Error	94
A.3.2	Spectral angle mapper	94
B	APPENDIX: ORIGINAL PUBLICATIONS	97

1 Introduction

Three centuries ago Sir Isaac Newton proposed the concept of dispersion of light, indicating that white light can be dispersed in continuous colors using prisms [1]. The color of an object is a continuous function of wavelength of electromagnetic radiation. The radiation comes from the object due to reflection, transmission or the object's irradiance itself [2]. The human eye can sense electromagnetic radiation around 380 *nm* to 780 *nm* as a visible light. Figure 1.1 shows the color spectrum of visible light in electromagnetic radiation. Human eye interprets the electromagnetic radiation around wavelength 400 *nm* as blue color, similarly around 550 *nm* and 700 *nm* as green and red color. The change of color in visible light according to wavelengths have been depicted by color spectrum as shown in Figure 1.1. The invention of the charged coupled device (CCD) detector in 1969 allowed optical image data to be transformed into an electronic format on which one can apply digital electronic processing techniques [1]. Most display devices are capable of showing three channels Red, Green and Blue (RGB). But three-dimensional color representation may not be enough for fully understanding color and its management [3] since color is the continuous function from 380 *nm* to 780 *nm* of wavelengths. Just by approximating the color from three-channels, we may lose information if the color signal has a lot of picks and discontinuities, as an example in fluorescent light [4]. Similarly, in case of metamerism, the colors may look same to the eye or sensor system when the spectra are different [5,6]. Metamers arise because the number of degrees of freedom in the sensor system, three for the cones in the normal human eye or a typical camera, is smaller than the number of degrees of freedom needed to specify different spectra [5,7]. As a result, metamerism is a serious limitation of tristimulus based representation and reproduction systems. A RGB model does a poor job of representing the wide spectral variation

of spectral power distribution and surface scattering properties that exists in the real world [8]. Therefore, color should be represented by an n-dimensional spectrum [3], here n-dimension is the number of bands or wavelengths used to represent or capture the colors and is assumed to be distinctly larger than three.

The use of spectral color is increasing [6]. Internet hits and database searches of hyperspectral images (the term hyperspectral or multi-spectral are used for spectral image in remote sensing [3]), a subset of spectral images, have been increasing exponentially in recent years [9]. The spectral image is a digital color image with wavelengths' spectrum at each pixel [10]. The spectrum is measured for a large number of narrow bands, unlike the three bands in a RGB-image. Figure 1.2(a) shows the spectral image as a set of band images of different wavelengths, and Figure 1.2(b) shows the spectrum gathered from a pixel. Spectral technology was developed long time ago, but until the early 1990s it was mainly used in astrophysics, remote sensing and terrestrial military applications [11,12]. Its application has been widened in various fields, some of the leading fields being archeology and conservation, medicine, pharmacology, agriculture, forestry, food engineering, environment, remote sensing as well as many more [11,13–17]. Spectral imaging produces a huge set of data, but the exploitation of multi-core processors and graphical processing units make spectral image processing possible in real time [18–21].

The objective of the thesis is to perform a study of different types of colored surfaces, ranging from the diffuse surface of a pigment coated plastic, to highly glossy surface of metallic and pearlescent coatings, as well as surfaces that are affected by the highlight effect. In this thesis a method to simulate the reflectances of diffuse plastic surfaces according to the concentrations of the pigments has been presented. The method also predicts the concentrations of suitable mixed pigments and their reflectances, given that the reflectance of the mixture is provided. This method has been called spectral color mixing and unmixing. Similarly, a reflectance prediction method for the simulation of the reflectances

Introduction

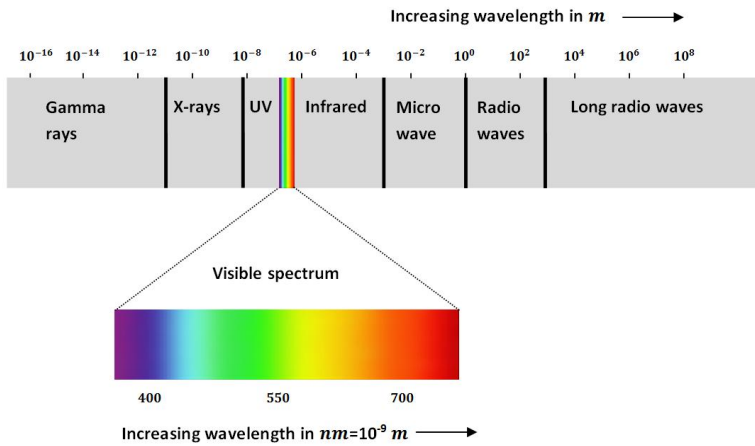


Figure 1.1: The electromagnetic spectrum. Colors in visible spectrum shows the interpretation of visible light as color by human eye according to wavelengths.

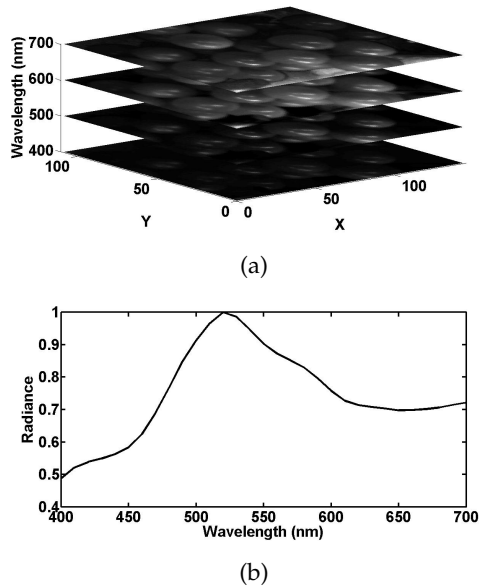


Figure 1.2: Spectral image representation (a) Spectral image shown in different bands. (b) Spectrum of a pixel. The spectrum has higher values between 500nm to 550nm, so human eye sense this spectrum as green color (please look at Figure 1.1).

of metallic and pearlescent samples has been developed. The first step in the method is to decide the best viewing angles, followed by the prediction of reflectance in all viewing angles by using the reflectance from a few best viewing angles. This method has been called reflectance prediction in multi-angle measurement. The reflection from the surface of the highlight-affected image (specular-affected image) has been separated into diffuse and highlight components. Highlight removal has been conducted on the RGB image and spectral image. The method is capable of simulating the color and reflectance of diffuse components from RGB and spectral images respectively. Throughout the thesis this method is called the highlight removal method.

In the spectral color mixing and unmixing method, the traditional Kubelka-Munk (KM) method has been used. But the KM method is only suitable for diffuse rough surfaces and is not capable of producing a prediction model for glossy surfaces like metallic and pearlescent samples. For glossy surfaces metallic and pearlescent coated surfaces have been chosen. In that part of the research, instead of analyzing the reflectance prediction in pigment mixing, reflectance prediction for different viewing angles has been carried out. Principal component analysis and the Wiener estimation method have been utilized to obtain the reflectance in different viewing angles. Spectral color mixing and unmixing and reflectance prediction in multi-angle measurement have been conducted by measuring the single representative reflectance at a point on the surface. The full image has been used as the input in the highlight removal method. Highlight and diffuse components from the image have been separated from a single image. The method is based on the dichromatic reflection model. For the RGB image, PCA and histogram equalization have been used to separate the highlight and diffuse components of the image. Similarly, for the spectral image, the positive constrained and sum to one spectral unmixing method have been used to separate the highlight and diffuse components of the image.

In the experiments in this thesis, the spectral image has been

exploited for the visible range within the wavelengths of 380 *nm* to 780 *nm*. The spectra, measured by an Avamouse handheld reflection spectrometer with an annular measuring geometry of 45° under circular illumination in the visible range of 380 *nm* to 750 *nm* with 5 *nm* sampling [22], has been used in the spectral color mixing and unmixing process. A Hamamatsu Photonic Multichannel Analyzer has been used in multi-angle measurement to measure the spectra within 380 *nm* and 780 *nm* with sampling of 5 *nm*. In the highlight removal method, the spectral image has been measured by a liquid crystal tunable filter (LCTF) [23] and Hypsux VNIR-1600 pushbroom camera [24]. LCTF measures the reflectance within the range 420 *nm* to 720 *nm* with a sampling of 10 *nm*. Similarly, a Hypsux VNIR-1600 pushbroom camera measures from 400 *nm* to 1000 *nm* with a sampling of about 3.7 *nm*, producing 160 bands. The different cameras were chosen according to the experimental requirements. Spectral color mixing and unmixing were tested for the pigments coated on a round shaped plastic pipe, which makes a camera with a small aperture suitable for the purpose. Similarly, in multi-angle measurement the camera should be rotated to capture the spectra at different viewing angles, making a small-sized Photonic Multichannel Analyzer suitable both in handling and obscuring the less illuminated direction. In the highlight removal method from spectral image, different types of detector have been used, not with the intention of comparing the quality of the output of the image by different types of camera but to test the highlight removal method on spectral images acquired by different sources.

The thesis has been divided into seven chapters and a collection of articles. Following the introduction in *Chapter 1*, the research problems have been mentioned in *Chapter 2*, the basics of reflection have been described in *Chapter 3*. Spectral color mixing and unmixing have been described in *Chapter 4*. Multi-angle measurement has been presented in *Chapter 5*. *Chapter 6* describes the highlight removal method from a single image in both a RGB and spectral image. The conclusions and discussion section of the thesis are presented in *Chapter 7*, which is followed by the supporting articles.

2 Research Problems Addressed in this Thesis

The research problems in this thesis are as follows:

- In industrial color management, an analytical color mixing trial process is required. The analytical base trial process is expensive and time consuming. In analytical process, the type of pigments and its concentrations are selected on trials and every time after coating on the substrate, color matching verification is done. And the process is repeated until the desired match is obtained. The research goal is to reduce the expensive analytical base trial process in industrial color management. To achieve this goal, the color mixture from a given set of mixing pigments should be predicted, and the mixing pigments and its concentrations from the given pigment should also be predicted. The pigment color has been coated on a round shape plastic surface.
- In the metallic sample the reflectance of the surface varies according to the viewing directions. Furthermore, in the pearlescent sample the reflectance of the surface varies according to viewing direction as well as the illumination directions. It is always time consuming to measure reflectance in all viewing angles and illumination angles. In this research, the goal is to predict the reflectances in all viewing angles by using the reflectance measured from a few best viewing angles. First, the set of the few best viewing angles should be determined so that the predicted versus measured error is minimized.
- Highlights on the surface obscures the information and acts as a false object. Therefore, highlights should be removed before image processing and its analysis to obtain the correct

result. Here the goal is to remove the highlights from a single image. The dichromatic reflection model defines each pixel's intensity value as a diffuse component and highlight component. So the challenge is to remove the highlights from a single image without knowing the illumination information. A highlight removal methods for both RGB and spectral images have been developed.

The research problems were addressed as follows:

- A spectrometer with a small aperture was chosen as the measurement device to work together with the round shape of the plastic surface. The reflectance of eleven different pigments, with seven different concentrations of each pigment, were procured as the training data. From these eleven different pigments, the representative unit ratio of absorption and scattering coefficients of each pigment were calculated. By using the single constant Kubelka-Munk method, the reflectance of the mixture of known mixing pigments could be calculated. The linear least square method was employed to calculate the concentrations of mixing pigments. The best mixing pigments are those that produce the least reflectance error calculated against the reflectance of the mixture pigments. The method gives the different options of mixing pigments to produce the same mixture pigments. This flexibility helps reduce the cost of pigment production. The method has been used for the coating of the pigmented opaque plastic surface.
- The reflectance of different metallic and pearlescent samples were measured as training sets. The number of best viewing angles was decided according to fidelity values calculated from the training sets. First, the best viewing angles were determined by using the suboptimal method. The reflectance measured for a few viewing angles was used to predict the reflectances in all viewing angles by using principal component analysis. Beforehand, eigenvectors were calculated from the training data measured for all viewing angles. The dimension

of each eigenvector is the number of possible viewing angles. Therefore it is possible to predict the reflectance in angles that lie in the outer bound of the few best viewing angles. The results were improved using the higher order polynomial of the basis function in the Wiener estimation method.

- In the lab environment, highlights can be removed using a polarizer in front of the camera and light source during measurement. However this is not suitable for an image that has already been measured. Research has been done to remove the highlight from a single RGB as well as a spectral image. As a first step of highlight removal from a single RGB image, the highlight-affected area in the RGB image was segmented in the difference image between the given RGB image and its highlight free image. Histogram equalized first principal component was used in the reconstruction of the image from principal component analysis (PCA). The second principal component was discarded in the reconstruction process, if they were affected by the highlight. The reconstructed image from the PCA was improved by conducting transformation on the original part of image which was not affected by the highlight. The method does not need the light source information. Similarly, in the highlight removal from the spectral image, the highlight-affected area in the spectral image was first segmented using constrained energy minimization (CEM). One spectrum with a maximum distance value was chosen from the highlight-affected part as a endmember of the highlight. If the spectral power distribution (SPD) of the light source is known, SPD can be used as the endmember of the highlight. Similarly, endmembers of the diffuse part were chosen using an automated target generation program (ATGP). After determining the endmembers of the diffuse and highlight parts, the positive constrained spectral unmixing method was applied to find the abundance values of highlight and diffuse endmembers. After determining the abundance values of the diffuse and highlight endmembers at each pixel level,

the highlight and diffuse components were separated. The method was tested on a spectral image measured in the lab and on spectral images obtained from other sources.

The research problems mentioned and their solutions have been documented in scientific publications. The summaries of the publications are as follows:

In *Publication 1*, color mixing and unmixing methods based on the Kubelka-Munk method have been proposed. The method has been applied to the color of pigments situated on a plastic pipe. Since the plastic pipe is of a round shape, a camera device with a small aperture (AvaMouse) has been used to measure the samples. The proposed method is a spectral-based method, capable of predicting the reflectance of the pigments of a mixture. The novelty of the method is the concentration prediction of the individual mixed pigments from the mixture of pigments. The proposed method gives multiple options of a set of separate mixed pigments from the mixture pigments sorted according to the choice of different difference formulae. As a result, the cost effective pigments can be selected by monitoring the color difference to produce the required pigments. Finally, the method helps reduce the cost of pigment production.

In *Publication 2*, a set of best viewing angles has been proposed in multi-angle measurement for the set of metallic and pearlescent samples. The primary angles have been selected by analyzing the root-mean square error by the reconstruction process by principal component vectors. The number of primary viewing angles was chosen according to the number of eigenvalues that generate a cumulative contribution greater than 99.9 percent. By using the principal component vectors of the training set and the primary viewing angles, the reflectances in all viewing angles have been predicted.

In *Publication 3*, a set of best viewing angles have been proposed in multi-angle measurement for a set of metallic PVDF coating with mica, metallic PVDF coating with polyester and a pearlescent coating. The investigation found that number of primary viewing angles is three for the individual type and five for all types. The best

primary angles were determined according to the average minimum reconstruction error in the training set. The suboptimal sequential backward selection method was used to reduce the best primary angles to 10. Out of 10 primary angles the best primary angles were chosen using the full search method. This publication exploits the Wiener estimation method in the relation provided by PCA in the reconstruction. The publication reveals that as the order of polynomial of principal component increases up to the fifth polynomial order, the reconstruction error decreases.

In *Publication 4*, a novel method of highlight removal from a single RGB image has been presented. The novelty of the method is to calculate diffuse image without knowing the information of light source from single RGB image. The method has been tested on different types of RGB image, with textures and without textures, and some images have been directly downloaded from the Internet. The proposed method does not need prior information on the light source and the expensive task of color segmentation. In the method, the first principal component of the image has been applied by histogram equalization. In most of cases, the second principal component carries the highlight part of the image, but it is not true for all cases. Therefore, the second principal component is chosen or rejected according to a threshold value applied in the fidelity of the second eigenvalue. The reconstruction by PCA produces the highlight-free image, but the change in color value due to histogram equalized first principal component was noted. The color of the reconstructed image was corrected by using a second order polynomial transformation. The weight vector of the polynomial transformation was obtained using the transformation of the pixels of the reconstructed image to the original image corresponding to the highlight-free pixels in the original image.

In *Publication 5*, a novel method of highlight removal from a single spectral image has been presented. The highlight-affected part and diffuse part of the image have been segmented by CEM. The endmembers of the diffuse component were calculated from the diffuse segmented part using ATGP. The endmembers of the specular

part are the SPD of the light sources. The diffuse component and specular component of the spectral images were separated using the positive constrained spectral unmixing method. The number of required endmembers for the diffuse component was calculated using eigen analysis.

3 Light Surface Interaction

The spectral property of light is defined as a function of wavelength λ [10]. Spectrum $f(\lambda)$ corresponds to the physical quantity. If the function $f(\lambda)$ is concentrated in a small neighborhood around the mean wavelength λ_0 , the wavelength is monochromatic [10]. In the spectral capturing process, the light should be decomposed into spectral parts using filters, prisms or gratings and finally captured by a detector. The physical value that is measured by a radiation detector is proportional to the time average of the quadratic amplitude of the incoming radiation. It is a measure of radiation energy in a central spectral interval reaching the detector during the integration time and also of brightness [10]. In a line scanner camera [24] the spectra of one line are detected each time. The spectrophotometer-like device detects the spectra of a single point at a time.

3.1 REFLECTION MEASUREMENT

The color of the diffuse surface does not depend on the geometry of the measurement. Therefore it is enough to measure in one viewing angle and one illumination angle in order to characterize the surface reflection of the diffuse surface. Traditionally it is measured by *diffuse*[°]/*0*[°] and *45*[°]/*0*[°] geometry. In *diffuse*[°]/*0*[°] geometry, the sample is illuminated from all angles using an integrating sphere and the detector is at an angle near the normal to the surface. Similarly, in *45*[°]/*0*[°] geometry, the light source is at *45*[°] from the normal and the detector is at the normal to the surface. The measurement geometries have been shown in Figure 3.1. There are some materials like metallic and pearlescent, for which the reflection characteristics depend on the measurement geometry and required goniometric measurement as shown in Figure 3.2. The direction of illumination and observation have been shown by notations *i* and *r*, respectively and the surface normal of the measured sample is shown by nota-

tion n . The angles θ_i and ϕ_i are the zenith and azimuthal angles of the illumination direction (incident direction), respectively. The observation angle (viewing angle) is represented as in illumination direction by replacing suffix i with r . The metallic sample can be measured by fixing the light source but varying the viewing angles. But the pearlescent samples should be measured at different viewing angles for different illumination angles.

The reflection from the surface can be modeled by the bidirectional reflectance distribution function (BRDF) [25–27]. The BRDF of the surface at each wavelength is the ratio of a reflected radiance to the incident irradiance at each wavelength λ as shown in Equation (3.1.1).

$$BRDF(\lambda, \theta_i, \phi_i, \theta_r, \phi_r) = \frac{L(\lambda, \theta_i, \phi_i, \theta_r, \phi_r)}{E(\lambda, \theta_i, \phi_i)} \quad (3.1.1)$$

In Equation (3.1.1), L is the reflected radiance per unit of area, wavelength interval and solid angle. E is the incoming irradiance per unit of area and wavelength interval. Other notations are as described above for Figure 3.2.

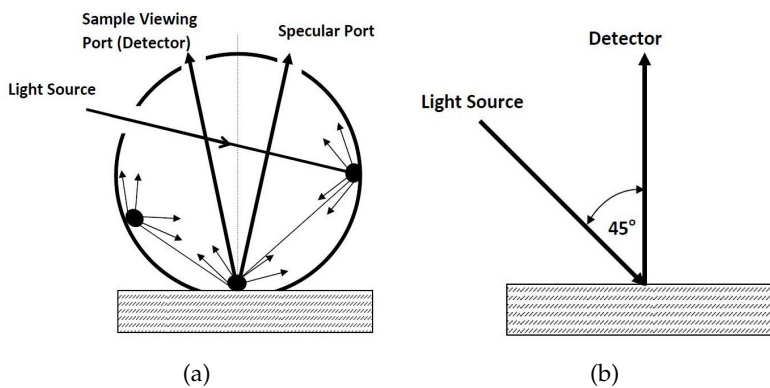


Figure 3.1: Measurement geometry (a) Diffuse°/0° geometry (b) 45°/0° geometry.

3.2 REFLECTANCE CALCULATION

The physical data on reflection that obtained from the device is the radiance of the surface. The radiance of the surface is converted into reflectance by dividing it by the radiance value of the white reference. The reflectance of the surface R_λ at each wavelength λ is supposed to be independent of the light source. The offset due to dark current is compensated by subtracting the radiance of the dark surface [25]. But in practice the radiance of dark surface is measured by entirely closing the light source and blocking any light from entering the lens. Equation (3.2.1) gives the reflectance of the surface relative to white surface used. The reflectance is independent of the illumination and sensitivity of the detector.

$$R_\lambda = \frac{\text{sample}_\lambda - \text{dark}_\lambda}{\text{white}_\lambda - \text{dark}_\lambda} \quad (3.2.1)$$

If the reflectance factor f_λ of the available white reference surface with respect to the perfectly diffuse lambertian white surface is

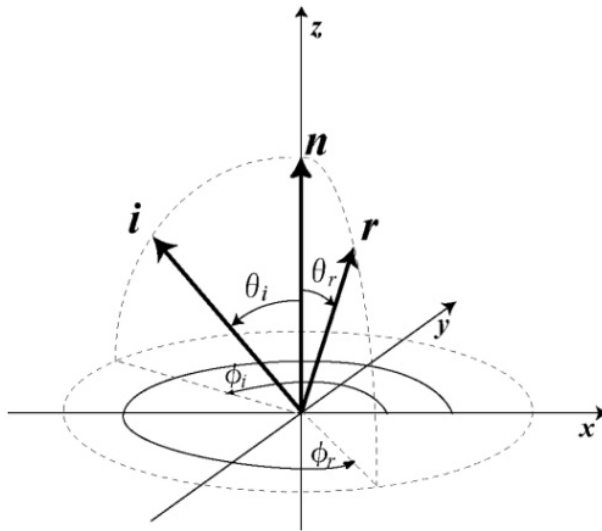


Figure 3.2: Multi-angle measurement geometry. Figure is adopted from reference [28].

known, Equation (3.2.1) is written as follows.

$$R_{\lambda} = \frac{sample_{\lambda} - dark_{\lambda}}{white_{\lambda} - dark_{\lambda}} f_{\lambda} \quad (3.2.2)$$

Here $sample_{\lambda}$, $white_{\lambda}$ and $dark_{\lambda}$ are the radiance values at each wavelength of the measured sample, white and dark reference respectively. Similarly, f_{λ} is the reflectance factor of the white reference. The reflectance factor of the white reference is the ratio of the radiance of the white reference to the ratio of the perfectly diffuse Lambertian white surface. Equation (3.2.2) has been extended for multi-angle measurement as follows.

$$R_{\lambda}(\theta) = \frac{sample_{\lambda}(\theta) - dark_{\lambda}(\theta)}{white_{\lambda}(\theta) - dark_{\lambda}(\theta)} f_{\lambda}(\theta) \quad (3.2.3)$$

The method as in Equation (3.2.3) has been used in the experiment in multi-angle measurement. Here θ is the viewing angle. The radiance of the white reference was measured for all viewing angles as the samples were measured. Throughout the thesis reflectance should be considered to have been calculated as described above.

3.3 DICHROMATIC REFLECTION MODEL

When light meets some part of the material it gets split into two. One part is directly reflected from the surface, which is the process of surface reflection. In surface reflection, the angle of incidence and the angle of reflection measured against the normal of the surface are equal. Another part enters the material, interacts with it, some of it passes through and is scattered and refracted by the material and finally exits from the surface through which it entered. This is the process of body reflection. Metal tends to reflect about 90% of incident light at the surface and appears highly shiny but colorless. In non-conductors such as dielectrics, a large proportion of the incident light interacts with the material, causing the body reflected light to have a specific color. In general terms, body reflection carries the diffuse component or color information of the surface and surface reflection carries the specular component or spectral distribution of the light source. Figure 3.3 shows the diffuse

component and specular component (highlight component) due to body reflection and highlight reflection in a dielectric material. As in Figure 3.3, part of the light is directly reflected, resulting in the specular component. Some remaining part of the light penetrates the surface of the translucent object and scatters due to interaction with the material and exits from different points at irregular angles, resulting in the diffuse component, and some part of the light is also absorbed; therefore 100% intensity of the light source cannot be measured from reflection.

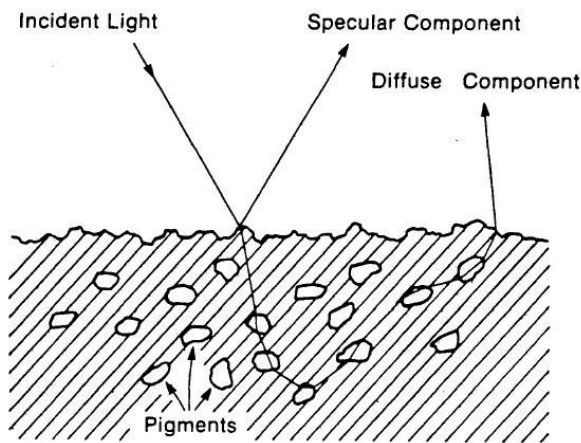


Figure 3.3: Reflection from an inhomogeneous surface with two components, specular and diffuse [29].

3.3.1 Formulation of Dichromatic Reflection Model

Shafer [30] described a dichromatic reflection model for modeling the reflectance of dielectric materials. Some examples of dielectric materials include porcelain (ceramic), glass, plastic, oxides of various materials, paints, tiles, vinyl, leaves and wood [31, 32]. The model suggests that the radiance spectra of the receptor is the linear combination of the diffuse and highlight components. Based on this model the response of the receptor for each wavelength λ at

geometric position (x) is defined as in Equation (3.3.1) [33].

$$R(x, \lambda) = d(x)R_d(\lambda, x)S(\lambda)q(\lambda) + s(x)S(\lambda)q(\lambda) \quad (3.3.1)$$

Where $R(x, \lambda)$ is the radiance value or response of the receptor at geometric position (x) at wavelength λ . The camera's sensor sensitivity at each wavelength is represented by $q(\lambda)$. $d(x)$ and $s(x)$ are the weighting factors for diffuse and highlight reflections respectively at each pixel position (x). The weighting factors are dependent on the geometric structure of the surface. $R_d(\lambda, x)$ is the diffuse reflectance or surface albedo at pixel position (x) and wavelength λ . $S(\lambda)$ is the spectral power distribution (SPD) of the illuminant. The specular component is the simple scaling of the illuminant, independent of the surface albedo [33].

In the case of a RGB image, the dichromatic reflection model for the single illuminant case is shown in Equation (3.3.2).

$$R(x, c) = d(x) \int_{\omega} R_d(\lambda, x)S(\lambda)q(\lambda)d\lambda + s(x) \int_{\omega} S(\lambda)q(\lambda)d\lambda \quad (3.3.2)$$

Here $R(x, c)$ is the color value of the receptor in the geometric position (x) and for color c . Here c represents either red, green or blue color. \int_{ω} represents the summation within visible range ω . The other notations are the same as for Equation (3.3.1). In a more general form, Equations (3.3.1) and (3.3.2) are represented in Equation (3.3.3).

$$R(x) = d(x)D(x) + s(x)S \quad (3.3.3)$$

Here $D(x) = \int_{\omega} R_d(\lambda, x)S(\lambda)q(\lambda)d\lambda$ and $S = \int_{\omega} S(\lambda)q(\lambda)d\lambda$ are represented for the RGB image at each color component. It should be noted that there are three different sensor sensitivity functions for individual red, green and blue color. The sensitivity function $q(\lambda)$ can be omitted from Equation (3.3.1) by merging it with the illumination term $S(\lambda)$, since the same sensor has been used even if the sensitivity is not flat [33]. Therefore, $S = S(\lambda)$ and $D(x) = R_d(\lambda, x)S(\lambda)$ have been represented for the spectral image at each wavelength.

3.3.2 Multiple Illuminations

The dichromatic reflection model can be extended to surfaces exposed to multiple illuminations. The SPD of the resultant light S^m is the summation of the SPD of mixed light S^i as shown in Equation (3.3.4).

$$S^m(\lambda) = \sum_{i=1}^L c^i S^i(\lambda) \quad (3.3.4)$$

Here c^i is the fraction of the SPD of mixed light. L is the number of mixed lights. Accordingly the response of the receptor for each wavelength λ at geometric position (x) is shown in Equation (3.3.5).

$$R^m(\lambda) = \sum_{i=1}^L d^i D^i + \sum_{i=1}^L s^i S^i \quad (3.3.5)$$

In Equation (3.3.5), L represents the number of exposed light sources. D^i is the radiance value of diffuse reflectance contributed to by the i^{th} light source and S^i is the SPD of the i^{th} light source. Accordingly, d^i and s^i are diffuse and highlight weighting factors corresponding to the i^{th} light source, respectively. Equation (3.3.6) represents Equation (3.3.5) in matrix form.

$$R^m = D^m d^m + S^m s^m \quad (3.3.6)$$

The superscript m is the representation of the case of multiple light sources. R^m is the response of the receptor and column matrix of size $n \times 1$. Here n is the number of wavelengths. $S^m = [S^1 S^2 \dots S^L]$ is the collection of SPD of L different light sources. Similarly, $D^m = [D^1 D^2 \dots D^L]$ is the collection of different diffuse spectra contributed by L different light sources. Since each radiance value at each pixel is of size $n \times 1$, the size of D^m and S^m is $n \times L$. The fractions of the diffuse component and highlight component are represented by $d^m = [d^1 d^2 \dots d^L]^T$ and $s^m = [s^1 s^2 \dots s^L]^T$ respectively. Each d^i and s^i are the scalar components resulting in a size of d^m and s^m to $L \times 1$.

3.4 DECOMPOSITION OF REFLECTION

As described in the dichromatic reflection model, the reflection from the material is the linear combination of body reflection and surface reflection. In the same fashion, in remote sensing the reflectance $R(x)$ at position x is defined as the linear combination of pure target signatures (endmembers) as shown in Equation (3.4.1) and the method is called spectral mixing and its decomposition is called spectral unmixing. Endmembers are the reflectance spectra of the pure materials.

$$R(x) = \sum_{i=1}^p a_i(x)e_i \quad (3.4.1)$$

In Equation (3.4.1), reflectance $R(x)$ is a combination of p number of endmembers. Where $a_i(x)$ is the fractional coverage called abundance of endmember e_i at pixel position (x) .

In color matching, reflectance R of the mixture of colorants A , B and C in quantities a , b and c is given in reference [34].

$$F(R) = aF(R_a) + bF(R_b) + cF(R_c) \quad (3.4.2)$$

Here R_a , R_b and R_c are the reflectance of the colorants A , B and C respectively. Absorption coefficient and scattering coefficient are defined as the function of reflectance in the two constant Kubelka-Munk method and the ratio of the absorption and scattering coefficient is defined as the function of reflectance in single constant Kubelka-Munk method applicable to an opaque surface. Details of the Kubelka-Munk method have been presented in *Chapter 4*. For p number of colorants, Equation (3.4.2) can be written as in Equation (3.4.3).

$$F(R) = \sum_{i=1}^p a_i(x)F(R_i) \quad (3.4.3)$$

Equations (3.4.1) and (3.4.3) are in the same mathematical form and can be solved by the same technique. The common equation for

both terms is written in Equation (3.4.4).

$$V = \sum_{i=1}^p a_i(x)E_i \quad (3.4.4)$$

Here notation V represents the mixture reflectance, a_i is the concentrations of each colorant in color mixing and abundance value in spectral mixing. E_i is the representation for e_i in spectral mixing and $F(R_i)$ in colorant mixing. The Equation (3.4.4) is represented in matrix form in Equation (3.4.5).

$$V = Ea \quad (3.4.5)$$

Where V is a column vector of size $n \times 1$, here n is number of bands. The size of matrix E is $n \times p$ and the size of the abundance or concentration matrix a is $p \times 1$. Here p is the number of mixing spectra, where the term spectra represents both reflectance and a function of reflectance. The value of a for each mixed spectra can be calculated quite easily by using the unconstrained linear least square estimation [35]. But the unconstrained linear least square estimation may give a negative value of abundance [36]. To restrict negative values and to get a percentage fraction, two constraints are usually imposed in Equation (3.4.1). These are the abundance non negativity constraint (ANC) and abundance sum to one constraint (ASC) as shown below.

$$a_i(x) \geq 0 \text{ for all } 1 \leq i \leq p$$

$$\sum_{i=1}^p a_i(x) = 1$$

The detail derivation of positive constrained factorization can be found in [37,38]. The positive constrained factorization was used to separate the highlight and diffuse components in *Publication 5*. The linear least square method was used to unmix the colorants from the given mixture in *Publication 1*.

4 Spectral Color Mixing and Unmixing

It is very important to choose the correct colorants with the correct concentrations to obtain the desired color of the surface. To get accurate results needs many expensive trials. The method proposed in *Publication 1*, describes a system that can be used to simulate the color obtained using certain colorants or the colorants to produce certain colors. Pigment mixing modeling by using full spectral calculation produces the more accurate results. Color mixing based on the Kubelka-Munk (KM) method [39] using full spectral calculation has been applied on the pigment coated plastic surface. The method is capable of calculating the required concentrations of the colorants to produce the desired color. The method can be used in quality management, a user measures the color of an object and the system tells them whether or not the color is acceptable by comparing the results to predefined color requirements. In addition, the method in *Publication 1* gives the choice of a set of colorants to the operator to produce the desired colors, according to quality requirements. This flexibility, as a whole, provides the advantage of producing the color within quality tolerances using different sets of colorants. It also provides the solution of color selection, without carrying out repeated expensive trials. As a result, production costs of the colorants can be reduced in the industrial process. The work in this chapter has been accomplished as a industrial collaboration with Exel. All the samples used in this experiment have been obtained from the Exel. By using the method, as described in *Publication 1* and in this chapter, we developed the software application, that has been successfully used in Exel for color mixing to coat on the top of curved plastic surface.

4.1 PREVIOUS WORKS

The method has been described which is applicable to all problems of color matching and which applies over the entire ranges of absorption [34]. In the method [34], it finds the functions of reflections and transmittance of colorants so that function of mixture colorants is the linear combination of mixing colorants. KM method gives relation of internal reflectance to the scattering coefficient S and absorption coefficient K [39]. The scattering coefficient and absorption coefficient of mixture have been assumed to be the linear relationship with that of mixing colors or of pigments [40]. The KM method has been used to determine optical properties of decorative and protective coating, paints, papers, pigmented polymers, fibers and wools, thermal insulations, biological systems, and in medical physics [41]. Saunderson correction converts the measured reflection by integrating sphere spectrophotometer including the specular component to the internal reflection on which the KM theory works [42]. Marcus and Pierce [43] propose the reflection correction for different measuring geometries. The revised KM theory [44] has been used for ink, paper and dyed paper. Different KM based methods have been used to find the optical characteristics of translucent paints [45]. Some of these methods are the black-white method [46], the inverse method [47], the infinite method [48] and the masstone-tint method [45]. Similarly there are a lot of work done for the color mixing using single constant KM method. Mainly single constant method is applicable to opaque paint surface and colored textile surface. Simplification of KM method to single constant KM method has been described in reference [49]. Paint approach method, textile approach method and hybrid method have been clearly described in that reference [49]. Many works have been done in color mixing by using color of three channels. As an example, Display monitors and color printers use RGB-based additive color mixing and CMY-based subtractive color mixing methods respectively [50,51]. Additive color mixing is only appropriate for additive colorants, such as colored lights [50]. Sub-

tractive color mixing by CMY accurately models the effect of light transmission through the color surface. As an example, if the white light, combination of red, green and blue, is transmitted through the cyan filter, then the red light is subtracted or absorbed, therefore only the green and blue light transmits. Similarly, magenta and yellow subtract or absorb green and blue light respectively. This CMY-based color modeling is used in color reproduction, like printing. RYB color space has also been proposed for paint-inspired color mixing [51]. CMY color modeling works best for purely transmitting materials, but it is insufficient for pigment modeling since pigmented surfaces have both transmitting and reflecting characteristics [50]. The most correct way of dealing with light is on a wavelength by wavelength basis [4,50,52]. Therefore, pigment mixing modeling by using full spectral calculation produces the more accurate results. Color mixing based on the Kubelka-Munk (KM) method [39] using full spectral calculation has been tested on the pigment coated plastic surface.

4.2 SAMPLE PREPARATION

In the experiment, eleven set of pigments with seven different concentrations were used. First, the seven different concentrations [0.2 0.5 1.0 2.0 4.0 6.0 10.0] in grams were dispersed in one liter of filling material and painted on a plastic pipe. The plastic pipes after coloration have been shown in 4.1. The plastic pipes were a circular pipe with small radius of about 1.5 cm, and therefore a spectrometer called AvaMouse [22] with a small aperture was chosen as the measurement device for the training and test sets. The AvaMouse spectrometer measures the reflection with an annular measuring geometry of $45^\circ/0^\circ$ under circular illumination in the visible range of 380 nm to 750 nm with 5 nm resolution. The colors were accurately measured, regardless of the gloss and orientation of the texture [22]. At first the measured reflectances were converted to internal reflectances according to the formula for geometry $[45^\circ/0^\circ]$, as described in Section 4.4. The samples were measured with close

contact with the spectrometer so the difference after correction is not great. The corrected reflectances of all eleven pigments of the seven different concentrations have been shown in 4.2. For each set of training pigments, the unit k/s ratio was calculated beforehand and applied as the input for the training set in the computation for color mixing or concentration calculations.

4.3 KUBELKA-MUNK METHOD

The KM method is a two-flux approximation of the general radiation transfer theory in which the upward and downward fluxes are an average representation of all rays travelling toward the upper and lower directions [44]. The KM method assumes that light should be diffused, scattered up and down and should not be polarized to get acceptable results. The scattering and absorption coefficients of the pigments are assumed to be constant over the thickness. Reflectance of the pigment surface depends on its thickness, absorption and scattering coefficients of the film's material, and reflection from the substrate. The KM method does not consider reflectance in the boundary because of the difference between the refractive index between air and the medium [53]. Such reflectance is called internal reflectance. Some correction method is required to convert from measured reflectance to internal reflectance, or vice versa. Correction methods have been presented in Section 4.4. The reflectance from the pigmented material has been shown in Figure 4.3. The simplification of reflection as a two-flux approximation



Figure 4.1: Round shape plastic pipe coated with different color pigments.

Spectral Color Mixing and Unmixing

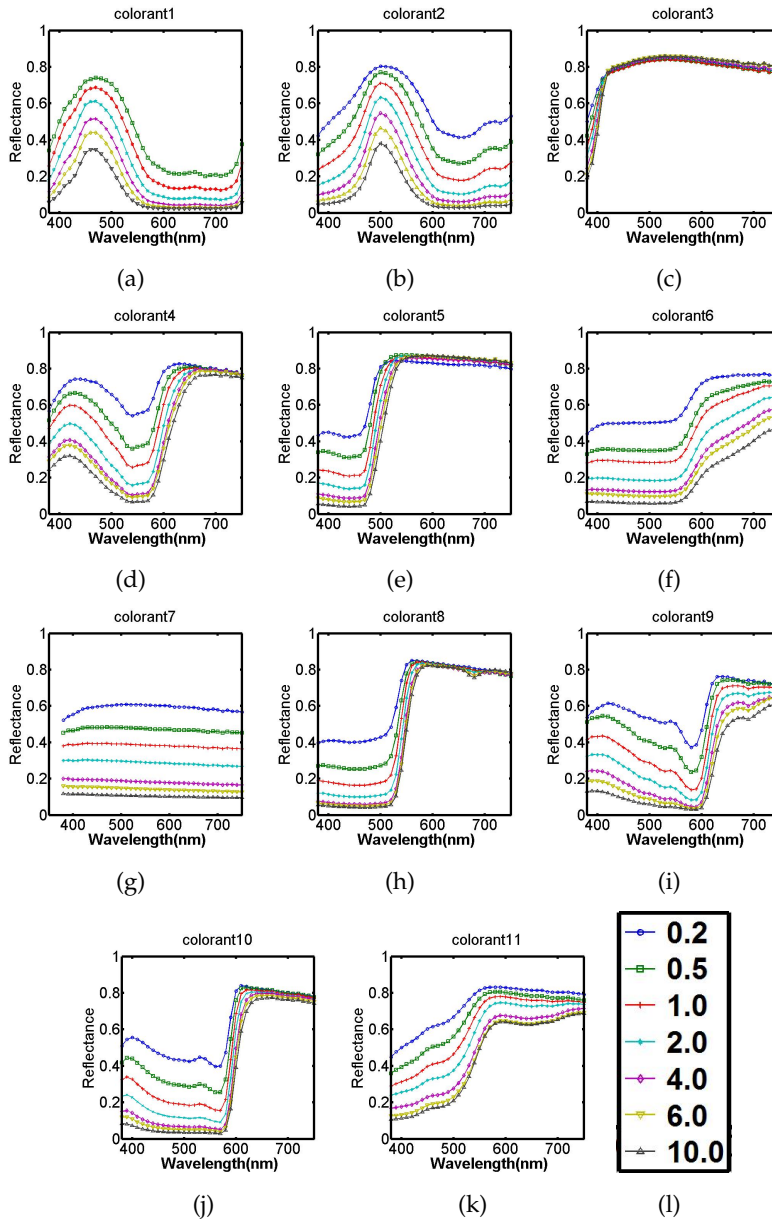


Figure 4.2: Figures from a to k show the reflectance of pigments in different concentrations and Figure l shows the legend representing all seven concentrations.

in the KM method applied to a pigment coated over a substrate has been depicted in Figure 4.4. In Figure 4.4, a pigmented solution is

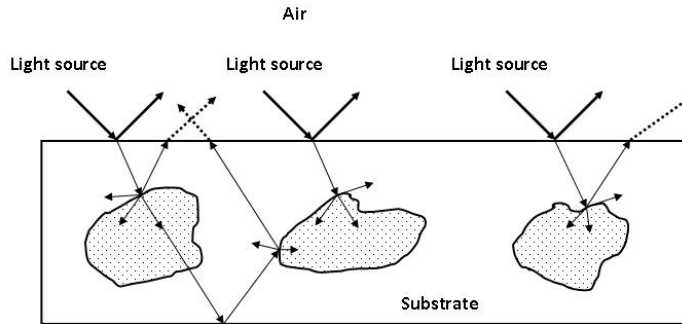


Figure 4.3: Reflection of light from pigmented material. Reflection shown by solid line is surface or specular reflection and reflection shown by dotted line is diffuse reflection due to scattering from filling materials and pigments. The reflection from substrate also produces the diffuse reflection

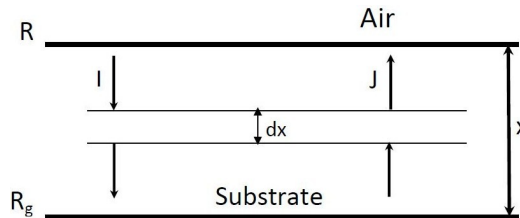


Figure 4.4: Schematic diagram of scattering and absorption of light energy inside a pigmented surface as used in the KM method [50].

coated on the substrate of reflectance R_g , the thickness of the coating is X . I and J are the intensities of the light travelling downward and upward to and from the substrate respectively. The downward intensities result from the scattering of the pigment and the source of the light. Similarly, upward intensities results from the scattering of the pigment and the substrate reflectance. The KM method simplifies the reflection model of the pigmented surface. The detail derivation of Equation (4.3.1) has been shown in Appendix A.1.

The reflectance R of the pigmented surface according to the KM

method is represented by the formula as shown in Equation (4.3.1).

$$R = \frac{1 - R_g(a - b \coth(bSX))}{a - R_g + b \coth(bSX)} \quad (4.3.1)$$

Where,

$$\begin{aligned} a &= 1 + \frac{K}{S} \\ b &= \sqrt{a^2 - 1} \\ X &= \text{Thickness of Coating} \\ R_g &= \text{Reflectance of substrate} \\ K &= \text{Absorption coefficient} \\ S &= \text{Scattering coefficient} \\ \coth &= \text{Hyperbolic cotangent} \end{aligned}$$

In the case of an opaque surface where the background is completely hidden, the film thickness X is assumed to be infinity ($X \rightarrow \infty$), because of that further change in the thickness do not affect the reflectance R [45]. So reflectance of substrate R_g has no effect on the reflectance of the opaque film, R_g is assumed to be zero ($R_g \rightarrow 0$). As a result, Equation (4.3.1) is simplified to Equation (4.3.2) for an opaque surface. Figure 4.6 shows the reflectance and its K/S value.

$$R = 1 + \left(\frac{K}{S}\right) - \sqrt{\left(\frac{K}{S}\right)^2 + 2\left(\frac{K}{S}\right)} \quad (4.3.2)$$

The ratio between the absorption and scattering coefficient K/S is obtained by reversing Equation (4.3.2).

$$\frac{K}{S} = \frac{(1 - R)^2}{2R} \quad (4.3.3)$$

4.4 REFLECTION CORRECTION

The discontinuity of refractive indices between the air and paint film (coating film) is not considered in KM theory [45]. The refractive index changes at the film/air coating interface. The change produces a significant optical effect that influences the color and appearance of the coating [43]. Therefore, the internal reflectance

by KM theory should be corrected to the measured reflectance, and measured reflectance should be corrected or converted into internal reflectance before calculating the optical characteristics of scattering and absorption coefficients. Reflection correction applicable to the KM method for the surface measured by integrating sphere (*diffuse*°/0°) and 45°/0° geometries have been presented [42,43,54].

The Saunderson correction is applicable to the reflectance measured by integrating sphere spectrophotometer including the specular component in the measurement [40]. The Saunderson correction [42] is used to calculate the internal reflectance as shown in Equation (4.4.1) [43,49].

$$R_{\lambda} = \frac{r_{\lambda} - K_1}{1 - K_1 - K_2(1 - r_{\lambda})} \quad (4.4.1)$$

Where, r_{λ} is the measured reflectance normalized between [0, 1] in each wavelength λ , K_1 is the fraction of incident light which is reflected from the front surface of the sample [42]. Only $1 - K_1$ of the incident light passes through the reflecting sample. The value of K_1 can be calculated as follows from Fresnel's law for normal incidence for a change in refractive index from n_1 to n_2 .

$$K_1 = \left(\frac{n_1 - n_2}{n_1 + n_2} \right)^2 \quad (4.4.2)$$

The value of K_1 is 0.04 for plastic, since plastic has a refractive index of 1.5 [40,53] and air has a refractive index of about 1 [43]. Similarly, K_2 is the fraction of light incident diffusely upon the surface of the sample from inside which is reflected, so that the fraction $(1 - K_2)$ emerges from the sample to the integrating sphere [42]. The value of K_2 should be calculated by trial and error. Generally the value of $K_1 = 0.04$ and $K_2 = 0.6$ are used in the Saunderson equation for diffuse illumination/near normal viewing spectrophotometer [43].

The internal reflectance calculated by the KM method is corrected to the reflectance equivalent to measured reflectance by integrating sphere spectrophotometer, including the specular component. The Saunderson correction has been shown in Equation (4.4.3).

Equations (4.4.3) and (4.4.1) are the reverse of each other to convert internal reflectance to measured reflectance and vice versa.

$$r_\lambda = K_1 + \frac{(1 - K_1)(1 - K_2)R_\lambda}{1 - K_2R_\lambda} \quad (4.4.3)$$

The measured reflectance by *diffuse*^o/₀^o geometry is converted to an internal reflectance by considering the gloss factor as shown in Equation (4.4.4).

$$R_\lambda = \frac{r_\lambda - (K_1 - G)}{(1 - K_1)(1 - K_2) + K_2(r_\lambda - (K_1 - G))} \quad (4.4.4)$$

Here G is the gloss factor that varies from 0 to K_1 from a perfect glossy surface to a perfect matt surface. In the case of perfect matt surface, Equation (4.4.4) is same as Equation (4.4.1). The corrected reflectance is converted to measured reflectance for geometry *diffuse*^o/₀^o by reversing Equation (4.4.4) as shown in Equation (4.4.5).

$$r_\lambda = (K_1 - G) + \frac{(1 - K_1)(1 - K_2)R_\lambda}{1 - K_2R_\lambda} \quad (4.4.5)$$

Similarly, the reflectance measured by 45°/0° measuring geometry is converted to internal reflectance as shown in Equation (4.4.6).

$$R_\lambda = \frac{r_\lambda}{T_1T_2 + K_2r_\lambda} \quad (4.4.6)$$

Here $T_1 = 0.095$ and $T_2 = 0.43$ are the transmittance across the air film boundary for a film with a refractive index of 1.5. The internal reflectance is converted to measured reflectance for geometry 45°/0° by reversing Equation (4.4.6), as shown in Equation (4.4.7).

$$r_\lambda = \frac{T_1T_2R_\lambda}{1 - K_2R_\lambda} \quad (4.4.7)$$

4.5 SPECTRAL COLOR MIXING

It may be assumed that K and S values for the individual pigments are additive in the mixture in proportion to the concentration of the pigments in the film [40], as in Equations (4.5.1) and (4.5.2).

$$K_m = c_1k_1 + c_2k_2 + \dots + c_nk_n \quad (4.5.1)$$

$$S_m = c_1s_1 + c_2s_2 + \dots + c_ns_n \quad (4.5.2)$$

Where k_i and s_i are the absorption and scattering coefficients of the i^{th} pigments at unit concentrations (100% concentration) respectively and are called unit absorption and unit scattering coefficients respectively. c_i is the concentration proportion of the i^{th} pigment where $\sum_{i=1}^n c_i = 1$. The subscript i varies from 1 to n , here n is the number of pigments used in mixing. K_m and S_m are the absorption and scattering coefficients of the mixture respectively. Equations (4.5.1) and (4.5.2) lead to Equation (4.5.3).

$$\frac{K_m}{S_m} = \frac{c_1k_1 + c_2k_2 + \dots + c_nk_n}{c_1s_1 + c_2s_2 + \dots + c_ns_n} \quad (4.5.3)$$

In the opaque surface, based on Equations (4.5.3) and (4.3.3), the reflectance of the mixture can be predicted when the pigment concentrations and unit absorption and unit scattering coefficients are known. The method is generally called the two constant KM method, since both the scattering and absorption coefficients are required. If the film is not opaque, the values of a and b in Equation (4.3.1) should be calculated after the calculating K/S value. The K/S value of the non-opaque film can be calculated by measuring the reflectance over the white substrate and black substrate [55].

In the opaque plastic surface, the scattering is mostly due to the filling material [40]. Therefore, scattering coefficients of pigments are replaced by the scattering coefficient s_w of the filling material. Suppose that $c_w = c_n$, $k_w = k_n$ and $s_w = s_n$ are corresponding representations of the filling material. The two constant KM method in Equation (4.5.3) is reduced to the formula as shown in Equation (4.5.4).

$$\begin{aligned} \frac{K_m}{S_m} &= \frac{c_1k_1 + c_2k_2 + \dots + c_wk_w}{c_1s_w + c_2s_w + \dots + c_ws_w} \\ &= \frac{c_1k_1 + c_2k_2 + \dots + c_wk_w}{s_w(c_1 + c_2 + \dots + c_w)} \\ &= \frac{c_1k_1 + c_2k_2 + \dots + c_wk_w}{s_w} \end{aligned} \quad (4.5.4)$$

Here $c_1 + c_2 + \dots + c_w = 1$, as the summation of all concentration fractions is 1. The equation is reduced as follows.

$$\left(\frac{K}{S}\right)_m = c_1 \left(\frac{k}{s}\right)_1 + c_2 \left(\frac{k}{s}\right)_2 + \dots + c_w \left(\frac{k}{s}\right)_w \quad (4.5.5)$$

Equation (4.5.5) is called the single constant KM method since knowledge of k/s of each pigments and its concentration are enough to predict the reflectance of the film.

The first step in color mixing in the single constant KM method is to calculate the unit k/s value of each pigment. The unit k/s is the ratio of absorption over the scattering coefficient when the 100 percent pigment has been used. The K/S value when a single pigment is dispersed in the filling material is given.

$$\frac{K}{S} = C_1 \left(\frac{k}{s}\right)_1 + C_w \left(\frac{k}{s}\right)_w \quad (4.5.6)$$

Accordingly, the unit k/s of the pigments dispersed in the filling material is calculated as shown in Equation (4.5.7).

$$\left(\frac{k}{s}\right) = \frac{\left(\frac{K}{S}\right)_{mix} - C_w \left(\frac{k}{s}\right)_w}{C_1} \quad (4.5.7)$$

Where,

C_1 concentration of pigment.

C_w concentration of filling material.

In an ideal case, the unit k/s of the pigment should be unique for each pigment but in practical experiments it was found that unit k/s varies as calculated from different concentrations, as shown in Figure 4.6. The normalized unit k/s value is used to check the correctness of the measurement. The large distortion in normalized unit k/s of the same pigments calculated from different concentrations reveals the incorrect measurement. Normalized unit k/s value can be calculated by dividing unit k/s value by its maximum value, as shown in Figure 4.6. The linear least square method can be employed to calculate the single representative unit k/s from the set of

unit k/s of same pigments mixed with filling materials in different proportions. The detailed formulation of the calculation has been shown in *Publication 1*. After knowing the unit k/s and concentration fraction of each mixed pigments in the mixture, the K/S value of the mixture should be calculated according to Equation (4.5.5). Finally the reflectance is predicted according to Equation (4.3.2). The reflectance and its color produced by mixing three color pigments have been shown in Figure 4.5. The Table 4.1 shows the differences between the measured reflectance of training sets and the reconstructed reflectance of training sets by setting the number of pigments one in mixture. The errors shown in each row are the average reconstruction error of all seven different concentrations of each pigment in the training sets. The Lab color difference formula was calculated by using daylight source (D65) and CIE 1931 standard observer.

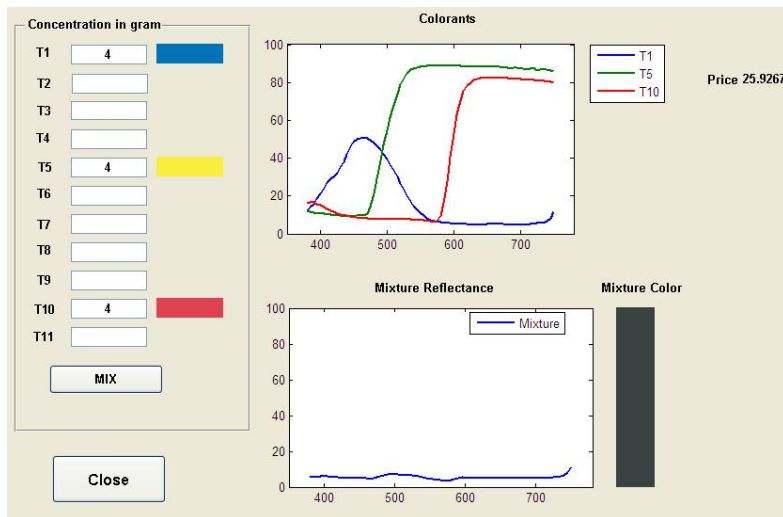


Figure 4.5: Spectral color mixing result using three colorants. Concentrations are in gram per liter.

4.6 SPECTRAL COLOR UNMIXING

In spectral color unmixing, the given reflectance of the mixture pigment is separated into the pigments that can be mixed to predict the given mixture pigment. First the training set has been prepared. The training set contains the unit k/s vector of each available type of pigment. Unit k/s of each pigment is calculated as described

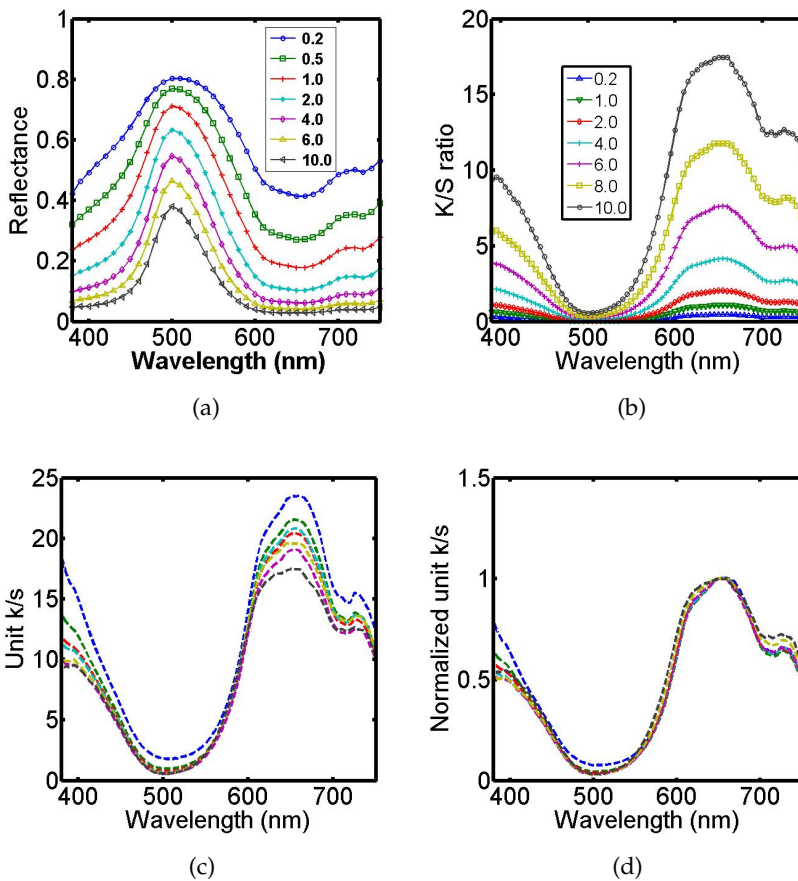


Figure 4.6: (a) Reflectance of pigments at different concentrations. (b) K/S ratio calculated from each reflectance. (c) Unit k/s calculated from each K/S. (d) Normalized unit k/s value, the large distortion in the shape of normalized unit k/s value reveals incorrect measurement.

above. In the first step, concentrations of the pigments in the mixture are solved. Then the reflectance of the mixture is predicted for all possible combinations. The combination of pigments which gives the less difference with a given mixture pigment form the pigments of choice.

Table 4.1: Error calculated between original samples and reconstructed samples. The results are the average values of all samples reconstructed in all seven different concentration by single constant method.

Sample no	MSE	GFC	CIELAB ΔE
T1	0.0001	0.9999	0.7813
T2	0.0003	0.9999	0.9052
T3	0.0002	1.0	0.81
T4	0.0006	0.9996	2.35
T5	0.0002	1.0	1.26
T6	0.0001	0.9998	1.248
T7	0.0004	1.0	0.68
T8	0.00020	0.9998	1.97
T9	0.0001	0.9999	1.52
T10	0.0001	1.0	0.72
T11	0.0023	0.9991	2.7

4.6.1 Concentration Prediction

The concentration of mixing pigments can be calculated, given that the unit k/s of each mixing pigment and K/S of the mixture pigment are known. The K/S of the mixture is directly calculated from the reflectance of the mixture, and the candidate unit k/s of the probable mixing pigments are selected from the training sets. Equation (4.5.5) can be written as a simple linear equation.

$$Y = XC \tag{4.6.1}$$

Where Y is the K/S vector of the mixture pigment. Let P be the number of bands in K/S . Then Y is the column vector of size $P \times 1$.

Assume that there are n number of pigments in the mixture, that means there are n number of unit k/s of each pigment. That makes $P \times n$ unit k/s matrix $X = [X_1 X_2 \dots X_n]$, here X_i is i^{th} unit k/s vector. The size of X_i is $P \times 1$. Assuming that C is the vector that contains the concentration fractions of each mixed pigment. The size of C is $n \times 1$. If X is assumed to be known then the problem remains to find C . The typical method to estimate C is the linear least square method. The form of estimation of the least square solution is the one that minimizes the estimation residual [35,37].

$$\underset{C}{\text{minimize}}(Y - XC)^T(Y - XC) \quad (4.6.2)$$

The least square solution can be done by using pseudo inverse calculation. The pseudo inverse solution of C is the following.

$$C = X^+ Y \quad (4.6.3)$$

Here X^+ is the representation of the pseudo inverse of matrix X . The pseudo inverse of the matrix is calculated as follows [35].

$$X^+ = (X^T X)^{-1} X^T \quad (4.6.4)$$

The predicted concentrations against the real concentrations have been shown in the Figure 4.7. The mixing pigments are not considered, if the pseudo inverse calculation gives a negative value. The Positive concentrations can be achieved by positive constrained and sum to one matrix factorizations [37,38]. The number of mixing pigments in the mixture can not be greater than number of bands of the reflectance.

4.6.2 Pigment Selection

The selection of the best set of mixing pigments from the pigments available in the training set to obtain the accurate pigment demanded is a challenging task in the painting process. The difference between the predicted pigment and the original pigment is calculated by the difference between the reflectances of these pigments.

Three different difference matrices have been used to calculate the similarity or dissimilarity between the original reflectance and predicted reflectance. One is a color-based method called CIELAB ΔE . The other two are spectral similarity measurements by using the goodness of fit coefficient (GFC) and the root mean square error (RMSE). GFC calculates the difference between the shape and does not depend on the magnitude of the spectra. But RMSE is like the Euclidean distance between two spectra. The details of the different formulae have been presented in the Appendix. To get the best selection of mixing pigments, the brute force approach has been used. The pigment combination that gives the least error with the desired pigment is the choice. First, concentrations of each pigment in every combination are calculated using Equation (4.6.4), then the reflectance of the mixture is predicted using Equation (4.5.5) for each combination. The work flow of the method of spectral unmixing is shown in Algorithm 1.

In the described method, different options of pigment sets are given to predict the desired signal, sorted according to the similarity between the predicted signal and desired signal. Figure 4.8

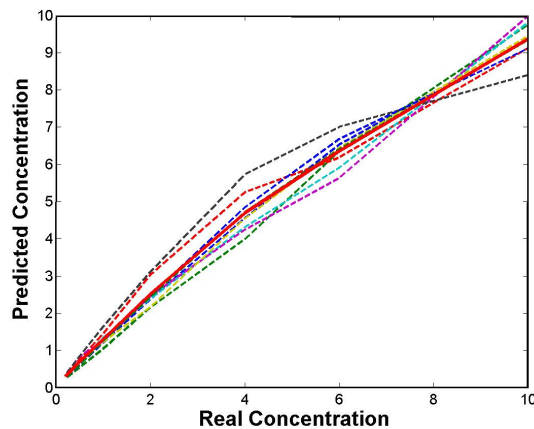
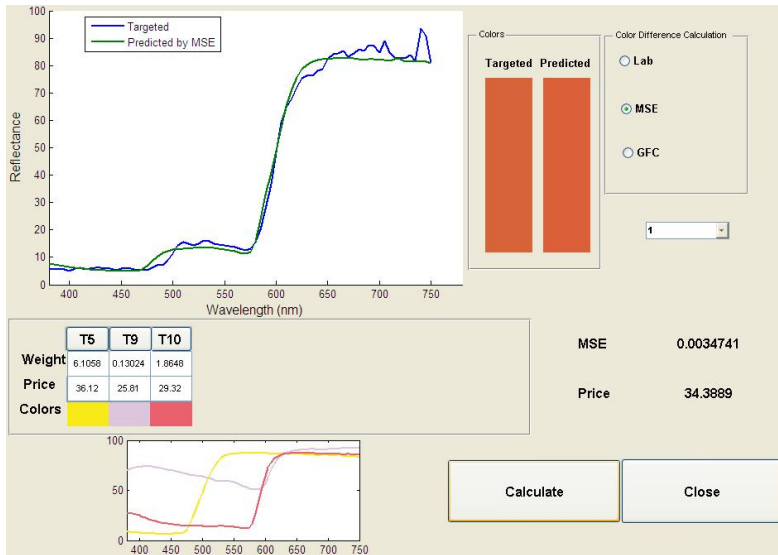


Figure 4.7: Real versus predicted concentrations in gram per liter. The solid line is the average of all concentrations. In ideal case each line should be straight line making 45 degree from the surface.

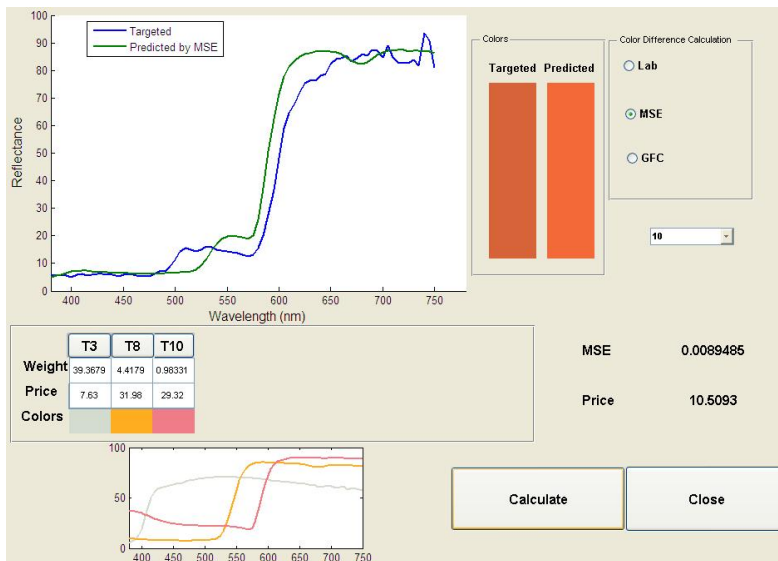
shows the unmixing results for first best result and tenth best result. The method gives option to the user to choose the result according to quality requirements. In that case the user can choose the colorants that have lower price and can check the quality of result. This process may reduce the cost of colorants. In the experiment eleven set of pigments with seven different concentrations were used. First the reflectance of all eleven pigments of the seven different concentrations have been collected from the round shape plastic pipe, as shown in Figure 4.1. The reflectances of the pigments in different concentrations have been shown in Figure 4.2. The reflectances were measured by an Avamouse handheld camera and corrected according to Equation (4.4.6).

4.7 DISCUSSION

In this section, KM method has been used to predict the reflectance of pigment mixture from given set of mixing pigments and its concentrations. Besides that, the method shows the capability of predicting the concentrations of mixing pigments and their reflectances. Single constant KM method has been exploited for that purpose and has been tested for the pigments coated on the curved plastic surface. The coating on the plastic surface has been assumed to be opaque. In this experiment the plastic pipe was curved, therefore spectral measurement was done by the device that has small aperture. The described method reconstructs the reflectance by using unit k/s value with high accuracy, $GFC > 0.999$. The results are summarized in Table 4.1. The described method can not be suitable for the translucent and transparent surface and as well as for the metallic and pearlescent coatings. The method should be extended to two constant KM-method to solve the problem for translucent and transparent coating surfaces. However, proposed method solves the problem of color mixing and unmixing for opaque surface and the developed method has already been in use by Exel.



(a)



(b)

Figure 4.8: Color separation of mixture and concentration prediction of mixing colors. Top figure shows the first best result and bottom figure shows the tenth best result. The price of the mixture has reduced drastically. T5, T9, T10, T3, and T8 are the name of training sets that are selected to produce given reflectance. The reflectance in small plot in each figure are the reflectance of selected mixing pigments in calculated concentrations.

Algorithm 1 Computational step to predict concentrations of mixing pigments.

1. Compute unit k/s ratio of each training set.
2. Convert reflectance of test set R_{mix} to K/S ratio using Equation (4.3.3).
3. Choose n number of pigments in mixture.

Repeats step 4 to 8 for all combinations.

4. Predict concentrations using Equation (4.6.3) and store row wise in matrix *concentration*.
 5. Negative concentrations and unexpected high concentrations are neglected.
 6. Predict $(K/S)_M$ ratio of mixture using predicted concentrations and unit k/s ratio from training sets, see Equation (4.5.5).
 7. Determine reflectance R_M using $(K/S)_M$, see Equation (4.3.2).
 8. Calculate difference ΔE between R_{mix} and R_M and store ΔE in array *error*.
 9. Order the matrix *concentration* according to array *error* sorted in ascending order for CIELAB color difference and MSE, and descending order for GFC.
-

5 Multi-Angle Measurement

Gonioapparent materials are material whose visual appearances changes according to illumination directions and viewing directions [56]. These materials are very important to the generation of many unique effects used in the printing of currency, the formulation of cosmetics and the application of paint mobiles [57]. In the mean time, it is necessary to determine the accurate reflectance of painted surface for the review of paint finishes before actual paintings in the exterior surface and for quality control for production and inspection process [56]. In this experiment, accurate reflectance prediction for gonioapparent coating in the form of metallic and pearlescent coatings is described. Integrating sphere and $45^\circ/0^\circ$ geometry as shown in Figure 3.1 have been traditionally used to measure the reflectance of diffuse surfaces, since the perceived chroma, hue and brightness are independent of the measurement geometry. Unlike diffuse surfaces, the perceived brightness of metallic surface depends on the viewing angle and is independent of the illumination angles, while the perceived chroma and hue are independent of the measurement geometry [57,58]. In addition, the perceived hue, chroma and brightness of pearlescent surfaces depend on both the viewing and illumination angles, unlike diffuse and metallic surface [57,58]. Therefore, reflectance measurement in different viewing angles is required to characterize a metallic surface. Similarly, different reflectance measurement in different viewing angles for different illumination angles are required to properly characterize the reflectance of a pearlescent surface. The optical principles of primary (first-order) interaction between light and three types of coated surface, diffuse, metallic and pearlescent, are summarized in Table 5.1. The work in this chapter has been accomplished as a industrial collaboration with Ruukki. All the samples used in this experiment have been obtained from the Ruukki. By using the method, described in *Publication 2* and *Publication 3*, we proposed

the method to find the best few viewing angles in multi-angle measurement so that we can reproduce reflectance in all viewing angles measuring only in few proposed viewing angles.

It is a time consuming and expensive process to measure the reflectance of gonioapparent coatings since it should be measured in different angles. In this research reference is made to *Publication 2* and *Publication 3*, in which the proposed method is capable of predicting reflectance in different viewing angles given the reflectance in a few view angles for metallic and pearlescent samples. In the experiment the illumination angle has been kept constant. First principal component analysis has been employed to predict the reflectance in different viewing angles for fixed illumination angles. The results by PCA outperforms the results by the cubic interpolation method. Wiener estimation method has been employed in the linear relation provided by PCA to get an improved result. The better results by the Wiener estimation method were achieved as the linear relation by PCA was extended to a higher order of polynomial. The outcome of the method reduces the time consuming experiments required in multi-angle measurement.

5.1 PREVIOUS WORKS

Different measurement angles have been proposed in the measurement of the metallic and pearlescent samples [53,56,57,59,60]. Three primary angles, one near specular at 15° , one far from specular at 110° and the third in-between at 45° for the measurement of the metallic surface were proposed [61]. Similarly aspecular angles of 20° , 45° and 70° were used to find better result than the previous geometry [59]. It was tested with both the metallic and pearlescent samples. Both methods used a polynomial modeling approach as the estimation method. Similarly the combination of primary angles 25° , 45° and 110° gave the highest correlation with the visual assessment for the metallic paint films [62].


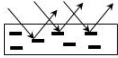
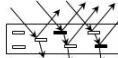
ASTM (American Society for Testing and Materials) recommends aspecular angles of 15° , 45° and 110° [53,60] for metallic samples.

Similarly, DIN (Deutsches Institut für Normung - German Institute for Standardization) recommends aspecular angles of 25°, 45° and 75° for metallic samples [53]. Aspecular angles of 15°, 35°, 45°, 70° and 85° viewing angles for an illumination direction of 15°, 45° and 65° have been proposed for pearlescent pigments [57]. Similarly aspecular angles of 10°, 18°, 28°, 40° and 90° viewing angles for an illumination direction of 60° have been proposed for all painted surfaces [56]. Principal component vector (PCV) was used to determine the best viewing angles and PCA method was used for prediction [56].

5.2 SAMPLE PREPARATION

In the first experiment, as described in *Publication 2*, altogether thirty different samples were used in the training set. Out of thirty

Table 5.1: Optical principles of diffuse, metallic and pearlescent coatings.

Pigment type	Diffuse	Metallic	Pearlescent
Optical principles of painting (first order)	 Diffuse scattering and absorption	 Specular reflection	 Thin film interference
Perceived brightness	Independent of geometry	Depends on viewing angles	Depends on viewing and illumination angles
Perceived chroma and hue	Independent of geometry	Independent of geometry	Depends on viewing and illumination angles

samples, nine samples were pearlescent and the rest were metallic. In the second experiment, as described in *Publication 3*, altogether there were forty-five different samples in the training sets. Out of forty-five samples twelve were pearlescent, twenty-one samples were metallic coated with PVDF with flakes, and six samples were metallic coated with polyester, and the remaining samples were metallic coated with PVDF. The reflectance of the metallic and pearlescent samples have been shown in Figure 5.1. The change in color in Figure 5.1 depicts the color transition according to the viewing angle. The reflectances of the objects were measured at

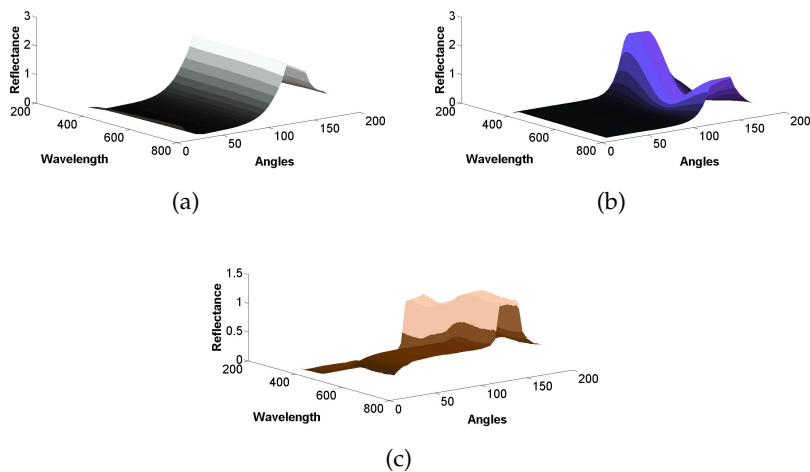


Figure 5.1: Reflectance of a) Metallic sample coated with PVDF with mica gray color b) Pearlescent c) Metallic sample coated with polyester. The light source is at 45° from the surface. Angles have been shown in a clockwise direction from the surface of reflection. The color change in the figures depicts the color transition according to the viewing angles.

different viewing angles using a Hamamatsu Photonic Multichannel Analyzer [63] within the visible range of 380 nm to 780 nm with 5 nm step under the light source halogen lamp with a $D65$ filter. The light source was set at 45° from the surface. The lab measurement setup has been shown in Figure 5.2. All the viewing angles are hereafter presented as aspecular angles unless otherwise stated. Aspecular angle is the angle measured considering the specular di-

Multi-Angle Measurement

rection as the reference point. For clarity, the aspecular angle in specular reflection has been shown in Figure 5.3. The samples were measured at 123 different viewing angles of 125° to 100° , 80° to 10° and -10° to -35° with one degree difference. Viewing angles from 135° to 124° and -36° to -45° were excluded from the measurement angles since the radiances emanating from the samples are near to zero and produce the noise. The angles between 101° to 79° were excluded from the viewing angles because the camera position obscures the light source. Similarly the angles between 9° to -9° were also excluded from the viewing angles since the radiances emanating from the samples became saturated due to specular reflection. The schematic diagram of the measurement setup is shown in Figure 5.4.

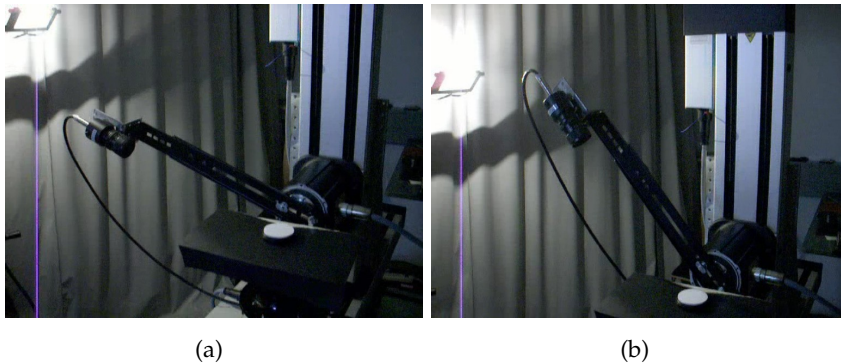


Figure 5.2: Multi-angle measurement setup, Light source is at 45° , detector has been shown in two different viewing angles.

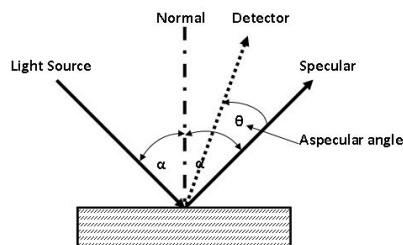


Figure 5.3: Aspecular angle representation in specular reflection.

5.3 MEASUREMENT ANGLES

In experimental investigation as described in *Publication 2*, We have proposed the first seven best primary angles for the prediction of reflectance of metallic and pearlescent samples for all viewing angles between aspecular angles of 125° to -35° , keeping light source at 45° from the surface. In that case, nine pearlescent samples and twenty one metallic samples have been used as training data. For the samples used and its measurement process , please look at Section 5.2 or *Publicatin 2*. The list of first seven best primary angles and their corresponding prediction errors are listed in Table 5.3. The samples were predicted by using PCA based prediction as explained in Section 5.4.1.

Similarly, In another experimental investigation as described in *Publication 3*, it has been found that only three primary angles are sufficient to predict the reflectance for all viewing angles between aspecular angles of 125° to -35° provided the estimation functions calculated from the training sets of similar types. Similarly five primary angles are sufficient to predict the reflectance in all viewing angles independent of the sample types. As described in Section 5.2, forty five samples were used as training set. All these samples were divided in three classes a) Pearlescent with twelve samples b) Metallic with PVDF coating with mica (Metallic 1) with twenty one samples c) Metallic coated with Polyester and PVDF with six samples of each (Metallic 2). In this experiment, improvement of

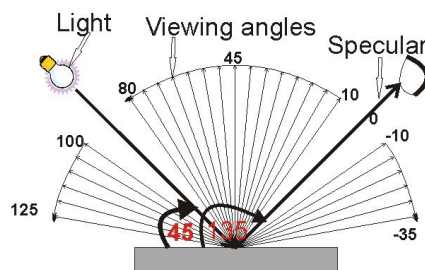


Figure 5.4: Schematic representation of multi-angle measurement, Light source is at 45° , detector has been shown in different viewing angles.

the the prediction error than as in described in *Publication 2* was observed by using the Wiener estimation in the higher order of polynomial in the relation provided by PCA as shown in Figure 5.6. Table 5.5 shows the best three viewing angles for individual type of samples and prediction errors. Similarly, Table 5.4 shows the list of best five primary angles and prediction errors accordingly.

5.4 PRINCIPAL COMPONENT ANALYSIS

Principal component analysis is useful to reduce the dimensionality of a data set, consisting of a large number of interrelated variables, while retaining as many variations as possible in the data set [64]. First the correlation matrix K of the data R is calculated. If data R is mean subtracted then the correlation matrix becomes the covariance matrix. The correlation matrix K is calculated as shown in Equation (5.4.1).

$$K = \frac{1}{c-1}RR^T \quad (5.4.1)$$

Here \square^T denotes the transpose of matrix. If the size of the matrix R is $r \times c$, as a result the size of the correlation matrix K is $r \times r$. Here r and c are number of rows and columns of the matrix R . In Multi-Angle measurement number of rows r is the number of viewing angles considered and the number of columns c is the number of measured items multiplied by number of wavelengths, if reflectance of all wavelengths were stored in R . Otherwise number of columns c is the number of measured items, if we consider different R for each wavelength. By definition, a correlation matrix is symmetric square matrix. From the symmetric square matrix, the basis function can be calculated by finding its eigenvalues and eigenvectors. For the correlation matrix K , the eigen equation $Kv = \sigma v$ is satisfied. v and σ are the eigenvectors and eigenvalues respectively of size $r \times r$. The eigenvalue σ is a diagonal matrix. The eigenvectors are the orthogonal matrix. The eigenvectors corresponding to the p largest eigenvalues are orthogonal basis function B . The size of the basis matrix B is $r \times p$. The proper number of eigenvectors as basis

functions were chosen according to the information content termed the fidelity ratio. The fidelity ratio f for the first p eigenvectors are calculated as the percentage of the sum of first p largest eigenvalues to the sum of total eigenvalues as shown in Equation (5.4.2).

$$f = \frac{\sum_{i=1}^p \sigma_i}{\sum_{i=1}^c \sigma_i} 100 \quad (5.4.2)$$

During the dimension reduction process, principal component P is calculated as in Equation (5.4.3).

$$P = B^T R \quad (5.4.3)$$

For an orthogonal basis function B , the elements of P are optimally mutually uncorrelated. The reconstruction of the data from the known basis function B and principal component P is calculated from Equation (5.4.4). The reconstructed error by PCA has been shown in Table 5.2.

$$R \approx \tilde{R} = B P \quad (5.4.4)$$

5.4.1 Prediction by PCA

Reflectance for all viewing angles can be reconstructed by the linear combination of first p principal components as shown in Equation (5.4.4). But the objective is to predict the reflectance for all viewing angles from the reflectance of the p number of primary angles of the test set. There is no known principal component of the test set, but only the basis function B (eigenvectors) is calculated from the training set. The matrix form of basis function B using the first p eigenvector sorted in descending order of eigenvalues is given below.

$$B = \begin{bmatrix} v_1(\theta_1) & \dots & \dots & v_p(\theta_1) \\ \vdots & \dots & \dots & \vdots \\ \vdots & \dots & \dots & \vdots \\ v_1(\theta_n) & \dots & \dots & v_p(\theta_n) \end{bmatrix}$$

First, principal component P_t is calculated using the basis function B and given reflectance of p number of primary angles. The principal component P_t is calculated as shown in Equation (5.4.5) [65].

$$P_t = b^T r \tag{5.4.5}$$

Here b is the matrix selected from basis function B according to the primary angles. r is the matrix of reflectance of the primary angles. The matrix forms of b and r are shown below.

$$b = \begin{bmatrix} v_1(\alpha_1) & \dots & v_p(\alpha_1) \\ \vdots & \dots & \vdots \\ \vdots & \dots & \vdots \\ v_1(\alpha_p) & \dots & v_p(\alpha_p) \end{bmatrix}$$

$$r = \begin{bmatrix} r_1(\alpha_1) \\ \vdots \\ \vdots \\ r_p(\alpha_p) \end{bmatrix}$$

Here, the primary angles are defined as $\alpha = (\alpha_1, \dots, \alpha_p)$ where the set of primary angles α should be the subset of total viewing angles $\theta = (\theta_1, \dots, \theta_p)$. After calculating the principal component, the reflectance in all viewing angles will be reconstructed using the basis function and principal component P_t . Here $r_i(\alpha_j)$ is $[r_i^{380}(\alpha_j) \dots r_i^{780}(\alpha_j)]$, if the prediction is done using the basis function calculated from the training set matrix R using all the wavelengths together. Otherwise $r_i(\alpha_j)$ is the reflectance value for each wavelength and P_t should be calculated for each wavelength. The calculation was done using all wavelengths together. i and j indicate the index of the principal component and primary angles respectively. The prediction of reflectance of the test sample for all viewing angles is achieved as shown in Equation (5.4.6).

$$R \approx \tilde{R} = B P_t \tag{5.4.6}$$

Figure 5.5 illustrates root mean square error (RMSE) due to PCA based prediction as described above and cubic interpolation. Seven

best primary angles have been used in prediction process. The results show that PCA based prediction clearly outperforms the cubic interpolation. Table 5.3 (on page 56) shows the prediction error by PCA using different viewing angles.

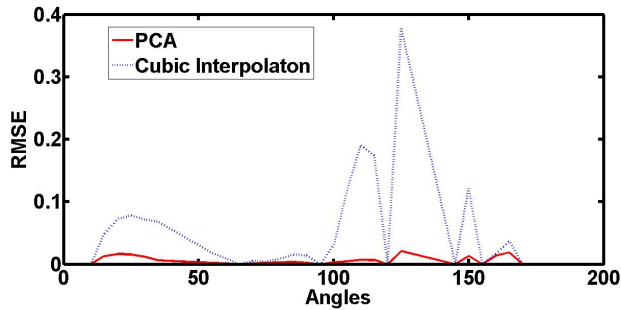


Figure 5.5: RMSE comparison of PCA based prediction and cubic interpolation. Here viewing angles in X-axis are measured from surface.

5.5 WIENER ESTIMATION

The Wiener estimation method is traditionally used to estimate data sets in larger dimensional space from lower dimensional space. In this study, this method has been employed to estimate the reflectance for all viewing angles from the reflectance for a few selected primary viewing angles. The Wiener estimation method is quite simple and provides accurate estimations [56].

The Wiener estimation rule to estimate the reflectance R for all viewing angles from reflectance r for a few primary angles with mapping function G is shown in Equation (5.5.1).

$$R = GP \tag{5.5.1}$$

Here P is the principal component calculated for reflectance r as shown in Equation (5.4.6). In Equation (5.5.1) the size of R is $n \times m$, size of G is $n \times p$ and size of P is $p \times m$. Here n is number of total viewing angles, m is the number of samples, and p is the number of

primary angles. If a single calculation was done for all wavelengths, then the new m is a product of the number of samples m and number of wavelengths k , $m = m * k$. The first order of the polynomial Equation (5.5.1) is exactly the same as Equation (5.4.4). The number of primary angles were selected according to the fidelity value calculated from PCA. The fidelity value chosen was ≥ 99.9 percent. The purpose of the estimation matrix G is to minimize the square error between the original R and estimated \tilde{R} [66].

$$e = | R - \tilde{R} | \longrightarrow \min$$

The estimation matrix G is explicitly represented in Equation (5.5.2) [66].

$$G = C_{RP}C_{PP}^{-1} \quad (5.5.2)$$

The notation $[\]^{-1}$ indicates the inverse of the matrix. Matrix C_{RP} is the cross correlation between matrices R and P . Matrix C_{PP} is the auto correlation of matrix P . The C_{RP} and C_{PP} are calculated as shown in Equation (5.5.3).

$$C_{RP} = \frac{RP^T}{m-1} \quad , \quad C_{PP} = \frac{PP^T}{m-1} \quad (5.5.3)$$

Here notation $[\]^T$ denotes the transpose of the matrix. As mentioned above, m is number of samples if individual calculations were done for each wavelength. Otherwise, it is the product of number of samples and number of wavelengths, if all the wavelengths were considered in single calculation. After calculating C_{RP} and C_{PP} , the estimation matrix G is calculated from Equation (5.5.2). After calculating estimation function G from the training set, the estimation of reflectance \tilde{R} for all viewing angles from the principal components P of the reflectance for particular primary angles are achieved from Equation (5.5.1).

In this experiment, the results were calculated using the first order polynomial to the fifth order polynomial of principal components. The predicted results improved considerably as the order of polynomial increased. The first order polynomial of principal component P of reflectance r for the three primary angles α_1 , α_2 and α_3

is arranged as $P_1 = [P_{\alpha 1} \ P_{\alpha 2} \ P_{\alpha 3}]$. In the second order polynomial for the three primary angles the new term $P_2 = [P_{\alpha 1} * P_{\alpha 1} \ P_{\alpha 1} * P_{\alpha 2} \ P_{\alpha 1} * P_{\alpha 3} \ P_{\alpha 2} * P_{\alpha 2} \ P_{\alpha 2} * P_{\alpha 3} \ P_{\alpha 3} * P_{\alpha 3}]$ is appended. Similarly the third order polynomial consists of the term $P_3 = [P_{\alpha 1} * P_{\alpha 1} * P_{\alpha 1} \ P_{\alpha 1} * P_{\alpha 1} * P_{\alpha 2} \ P_{\alpha 1} * P_{\alpha 1} * P_{\alpha 3} \ P_{\alpha 1} * P_{\alpha 2} * P_{\alpha 2} \ P_{\alpha 1} * P_{\alpha 2} * P_{\alpha 3} \ P_{\alpha 1} * P_{\alpha 3} * P_{\alpha 3} \ P_{\alpha 2} * P_{\alpha 2} * P_{\alpha 2} \ P_{\alpha 2} * P_{\alpha 2} * P_{\alpha 3} \ P_{\alpha 2} * P_{\alpha 3} * P_{\alpha 3} \ P_{\alpha 3} * P_{\alpha 3} * P_{\alpha 3}]$. So the second order polynomial $P = [P_1 \ P_2]$ and for the third order polynomial $P = [P_1 \ P_2 \ P_3]$ are used to calculate the estimation function. Similarly P can be arranged to a higher order of polynomials for a greater number of primary angles. From Equation (5.5.2) the estimation function G is derived. As the order of polynomial increases, the size of the estimation function increases accordingly. The prediction results up to the fifth order polynomial significantly improves. The results are shown in Figure 5.6.

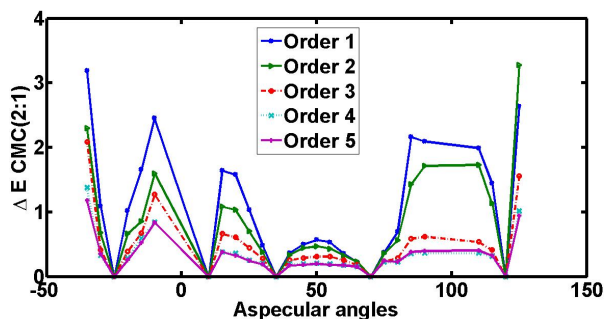


Figure 5.6: Prediction error by the Wiener estimation method using first to fifth order of polynomial using the five primary angles.

5.6 DISCUSSION

This section describes the PCA and wiener estimation based reflectance prediction in multi-angle measurement for metallic and pearlescent samples. In *Publication 2*, PCA based prediction method has been used. In PCA based method, thirty samples were used as training sets, Out of thirty samples, nine samples were pearles-

cent rest were metallic. Reconstruction from seven principal components contribute the fidelity ratio greater than 99.9. By checking fidelity ratio of training set, we proposed that seven best viewing angles are sufficient for the prediction process. Best viewing angles were selected depending on the minimum reconstruction error of training set. The results by proposed method outperformed the prediction of reflectance by cubic interpolation as shown in Figure 5.5. Similarly, reconstruction and prediction error by PCA are almost the same as shown in Table 5.2 and Table 5.3. Here reconstruction means the samples were reconstructed by PCA where we have reflectance of samples in all viewing angles but in Prediction we have reflectance of samples only in best viewing angles and PCV from the training sets. In *Publication 3* the wiener estimation based reflectance prediction in multi-angle measurement for metallic and pearlescent samples has been proposed. The wiener estimation was applied to the linear relationship provided by principal component analysis. The wiener estimation method up to the fifth order of polynomial of principal components has improved prediction results significantly as shown in Figure 5.6. The experiment shows that five best primary angles are sufficient to predict reflectance in all viewing angles independent of the types of samples. Additionally it has been found that only three best primary angles are sufficient to predict reflectance for all viewing angles using the estimation function calculated from the similar type of samples. The presented method takes into account only the single illumination direction at 45 degree from surface. Further test is required for choosing the best primary illumination directions and corresponding best primary viewing angles. The number of samples used for the training sets can not be enough for the samples that consists of the different types of color and glossiness. The number of samples used in training set may influence the required number of best viewing angles since the fidelity value may change but this does not matter so much since the presented method gives the set of best viewing angles combined from one best viewing angles to required number of best viewing angles.

Table 5.2: Reconstruction result by PCA: *Principal component vectors (PCV), total contributions (TC), mean values (μ) and maximum values (m) of CIELAB color differences (CIELAB ΔE), and Root mean square errors (RMSE) are shown.*

PCV	TC	Lab ΔE		RMSE	
		μ	m	μ	m
1 st	73.980	11.660	24.860	0.110	0.180
1 st -2 nd	90.99	5.620	14.044	0.054	0.130
1 st -3 rd	97.60	3.871	11.682	0.031	0.080
1 st -4 th	98.90	2.284	11.516	0.021	0.079
1 st -5 th	99.56	1.190	2.368	0.013	0.037
1 st -6 th	99.84	0.738	1.777	0.007	0.017
1 st -7 th	99.92	0.667	1.814	0.006	0.012

Table 5.3: Prediction from first seven best primary angles using PCA: *Mean values (μ) and maximum values (m) of CIELAB color differences (CIELAB ΔE) and the Root mean square errors (RMSE) are shown according to best angles.*

Best angles	CIELAB ΔE		RMSE	
	μ	m	μ	m
100°	9.350	18.970	0.101	0.171
50° – 30°	6.005	13.810	0.063	0.242
55° 25° – 20°	2.726	14.043	0.029	0.132
65° 25° 15° – 20°	1.968	13.406	0.019	0.092
125° 55° 30° 15° – 20°	1.074	3.633	0.013	0.082
125° 70° 40° 10° – 15° – 35°	0.733	2.530	0.008	0.051
125° 70° 40° 15° – 10° – 20° – 35°	0.603	2.501	0.006	0.021

Multi-Angle Measurement

Table 5.4: Prediction from five best primary angles using wiener estimation with fifth order of polynomials of PC: Mean values (μ) and maximum values (m) of color difference (ΔE CMC(2 : 1)) and the Root mean square errors (RMSE) are shown according to best angles for all type of samples.

Best angles	ΔE CMC(2 : 1)		RMSE	
	μ	m	μ	m
40°	6.863	12.287	0.133	0.442
70°20°	3.089	10.688	0.040	0.212
70°25° – 20°	1.425	5.262	0.020	0.116
70°30°15° – 20°	0.762	3.587	0.009	0.045
120°70°35°10° – 25°	0.309	1.177	0.004	0.022

Table 5.5: Prediction from three best primary angles using wiener estimation with fifth order of polynomials of PC: Mean values (μ) and maximum values (m) of color difference (ΔE CMC(2 : 1)), and Root mean square errors (RMSE) are shown according to the best three primary angles for each type of sample.

Sample type	Primary angles	ΔE CMC(2 : 1)		RMSE	
		μ	m	μ	m
Metallic 1	115° 25° –30°	0.458	1.515	0.008	0.038
Metallic 2	75° 20° –10°	0.384	1.263	0.005	0.012
Pearlescent	70° 20° –15°	0.498	2.902	0.007	0.023

6 Highlight Removal from Single Image

Highlight should be removed from the image to achieve the correct image processing results. If highlight is not removed it obscures the real feature and may give the impression of a required feature in the image, resulting in the incorrect image processing output. In fact, highlight is the artifact produced by the effect of the light source based on the viewing position. This chapter is about the highlight detection and highlight removal method from a single image, in both RGB and spectral images. Highlight detection is the method to find the part of area that is suffered from highlight and the highlight removal method removes the highlight from the image and produces the diffuse image. There may be the highlight free image (specular free image) without highlight but shifted color information. Here in this chapter, highlight removal method not only removes the highlight but also preserves the correct color or spectral information.

The highlight-affected image may produce a false result in stereo matching, segmentation, registration and detection in computer vision applications. In this chapter the goal is to provide the highlight removal method from a single image. The principal component-based technique for RGB images has been proposed in *Publication 4*, and the constrained spectral unmixing method for spectral images has been proposed in *Publication 5*. Some of spectral images with or without cross polarizer settings have been measured in the facility of Norsk Elektro Optikk As, Norway. Some test spectral images were obtained from Vladimir Bochko [67].

6.1 PREVIOUS WORKS

The starting point of the highlight removal method is the dichromatic reflection model as proposed by Shafer [30]. The dichromatic reflection model separates reflection into a diffuse component and specular (highlight) component when light meets the surface that is optically inhomogeneous. The dichromatic reflection model has been illustrated in Figure 3.3. Highlight can be removed from the image by using the cross setting of a polarizing filter in front of the camera sensor and light source during image acquisition. This is based on the idea that highlight or specular components are polarized and diffuse components are not polarized [68]. This polarizing filter method is not suitable for images that are already measured and it may not always be feasible to put a polarizing filter in front of the camera and light source. However the method can be used to test the quality of the measurements of the highlight removal algorithm.

Klinker *et al* [69] showed a T-shaped color distribution containing illumination and reflectance color vectors, but it may be difficult to get a T-shape in an image due to noise in the image. Tan and Ikeuchi [70] proposed a highlight removal method without color segmentation. The method first produces the specular free (SF) image. The specular free image is devoid of the highlight effect but saves the geometrical shape of the image. The highlight-free pixels are successfully detected by using the logarithmic differentiation between the SF image and input image. Then the specular component of each pixel was locally removed, involving the maximum of two pixels. Similarly, Shen *et al* [71] proposed a highlight removal method for a RGB image. The method does not need local interaction between two neighboring pixels and does not need color segmentation. The method solves the dichromatic reflection model on each pixel by solving the least square problem. Illumination-constrained inpainting method for highlight removal has been described in [72]. The method assumes that the illumination color is uniform throughout the highlight area. A fast highlight removal

method using iterative bilateral filtering method has been applied in RGB image by Yang *et al* [73].

There are fewer studies done on highlight removal from spectral images than from RGB images. Bochko and Parkkinen [67] propose a highlight removal method in spectral images using PCA. In the method, probabilistic PCA was used to detect the highlight-affected part and diffuse part in the image. Finally the highlight-affected part was mapped across the first eigenvector of the diffuse part. The method does not need prior information on the light source. However the quality of the diffuse image depends on the information that the first principal component carries. Similarly, there is a method to obtain a highlight-free image using the OSP method [33]. In the OSP method the radiance spectra should be projected on the subspace orthogonal to the spectra of illumination. Therefore, the OSP projector [33,74,75] rejects the uninteresting signature (spectra of illumination) from the input spectra and as a result a highlight-free spectra is achieved.

6.2 HIGHLIGHT DETECTION

The highlight-affected part and diffuse part in the spectral image were segmented using clustering in the first two principal component vectors [67]. A pixel clustering algorithm was presented to segment the diffuse and highlight parts [69], the results were demonstrated to work well for a set of plastic objects. The segmentation between diffuse and highlight parts were obtained by conducting clustering in two-dimensional histograms in spherical coordinates [31]. Here highlight detection methods for a RGB image as well as a spectral image have been presented. In the RGB image, the difference between the specular-free image and original image were first calculated, then the highlight and diffuse parts in the image were detected. For the spectral image, CEM-based highlight detection has been proposed.

6.2.1 Highlight detection in difference image

The highlight-affected area in the given RGB image is detected on a single pixel level, based on the difference between the original image and the modified specular-free image (MSF) [71]. The MSF is calculated by adding the mean of the minimum of the RGB color values in the original image to the specular-free image (SF) as shown in Equation (6.2.2). The SF is calculated by subtracting the minimum of RGB color value in each pixel level as shown in Equation (6.2.1).

$$SF_i(x) = I_i(x) - \min(I_1(x), I_2(x), I_3(x)) \quad (6.2.1)$$

$$MSF_i(x) = SF_i(x) + \bar{I}_{min} \quad (6.2.2)$$

In Equations (6.2.1) and (6.2.2), SF and MSF are the specular-free image and modified specular-free image. Similarly $I_i(x)$ is the value of i^{th} color channel at pixel (x) in original image I . The subscript i ranges from 1 to 3 corresponding to the Red, Green and Blue channel. \bar{I}_{min} is the mean of minimum of the RGB color values in the original image. The threshold value should be set to the difference between the original and MSF image to classify each pixel in the group of highlight and highlight-free parts as shown in Equation (6.2.3). The difference between original and MSF image at each pixel is shown in Equation (6.2.4).

$$pixel(x) = \begin{cases} \text{highlight} & \text{if } d_i(x) > th \text{ for all } i \\ \text{diffuse} & \text{otherwise} \end{cases} \quad (6.2.3)$$

$$d_i(x) = I_i(x) - MSF_i(x) \quad (6.2.4)$$

The average value of the minimum of the color channel has been used as the threshold [71]. However it is always a difficult task to set an accurate threshold value. The threshold value has been set after a visual assessment of the classification results of each image. The threshold value 0.1 has been set to detect highlight in the pear surface as shown in Figure 6.1. Instead of using a threshold, a simple K-means clustering [76] algorithm can be applied but it may

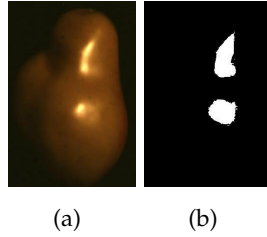


Figure 6.1: Highlight detection (a) Original Image (b) Black is diffuse part and white is highlight part.

compromise the speed of the processing. Similarly the SF image provided by other methods, like by Tan and Ikeuchi [70], can be used to calculate the difference image.

6.2.2 Highlight detection by CEM

CEM in an FIR filter [74] has been presented in *Publication 5* to detect the highlight in a spectral image. The method provides the optimal weight vector W , as shown in Equation (6.2.5) as derived by Frost [77].

$$W^T = \left(\frac{K^{-1}D}{D^T K^{-1}D} \right)^T \quad (6.2.5)$$

Where K is the autocorrelation matrix of the given image. D is the desired signature representing the specular component i.e. the spectra of the light source. The CEM filter, after applying an optimal weight vector W , is $W^T R$. The CEM filter is the fraction value of the desired signature at each pixel position, and as a result a one dimensional image is obtained. If R is the desired signature, then $W^T R = 1$. By applying the K-means clustering algorithm in the CEM filter, the highlight-affected part and diffuse part in the spectral image is detected as shown in Figure 6.2. Similarly, the highlight can be detected by performing clustering in the dataset plotted against the first principal component against second principal component [67].



(a)



(b)

Figure 6.2: Highlight detection by CEM (a) Original Image (b) Black is diffuse part and white is highlight part.

6.3 DIFFUSE IMAGE FROM RGB IMAGE

The section describes the highlight removal method from a single image without knowing the information about illumination. The method applies principal component analysis (PCA); histogram equalization in first principal component (PC). Analyzing the eigenvalue corresponding to the second PC, it decides whether the second PC contains the specular component. The method, as described in *Publication 4*, assumes that most of the highlight may be contained in the second PC. The second PC is selected or removed by determining whether or not it contains the highlight. The described method assumes that the highlight is not completely separated between different PC, still that there may be a highlight effect in the first PC. Histogram equalization was applied in the first PC to reduce the highlight effect.

The highlight-free image was obtained by reconstructing the im-

age by PCA. But the reconstructed result may have color difference with the original image. The new basis function was calculated by using second order polynomial transformation between the diffuse part of the reconstructed highlight-free image and diffuse part of original image. Finally, the calculated basis function was applied to the whole of the reconstructed highlight image by PCA to get the correct diffuse image. The second order polynomial transformation recovers the original color. The workflow of the method has been illustrated in Figure 6.4. Diffuse images simulated by using this method has been shown in Figure 6.3.

6.4 DIFFUSE IMAGE FROM SPECTRAL IMAGE

The diffuse image of a spectral image can be obtained by using the positive constrained spectral unmixing method, as described in *Publication 5*. In that method each pixel of the spectral image is defined as the combination of endmembers of different components. The known spectra of the light source can be the endmember of the highlight part, otherwise the spectra with large distance can be approximated as the endmember of the highlight part. Other endmembers for the diffuse part can be selected from the diffuse area by using the ATGP method. The required number of endmembers in the diffuse part can be selected by using eigen analysis. After obtaining all the endmembers, the positive constrained and sum to one spectral unmixing method is applied to calculate the abundances of each endmember corresponding to each pixel's position. Finally, the image should be reconstructed by using all endmembers, except the endmembers of the highlight component, to get the diffuse image. The benefit of this method over the OSP method is that the resultant spectra is always positive and preserves the shape of the spectra, and there is less color difference in the diffuse image. The results of the diffuse image has been presented in a three band image, as shown in Figure 6.5(d). The results of the spectra of the image from the highlight part have been shown in Figure 6.6.

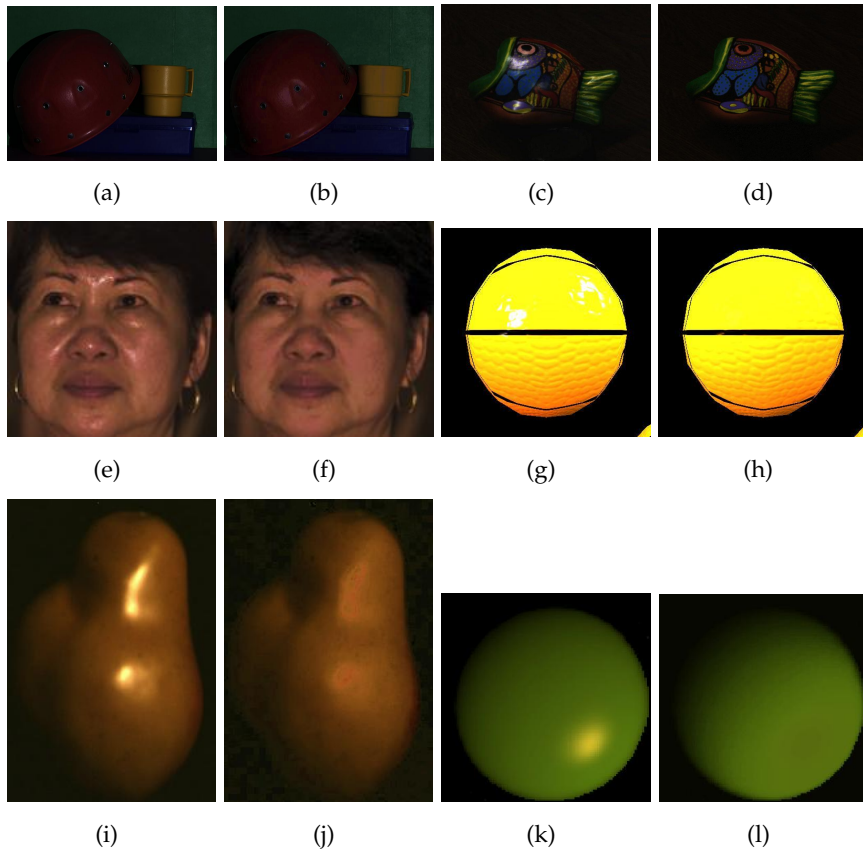


Figure 6.3: Highlight removal from RGB image (a,c,e,g,i,k) Original images (b,d,f,h,j,l) Diffuse images. The name of this images are called hat, fish, face, yellow ball, pear and green ball respectively.

Highlight Removal from Single Image

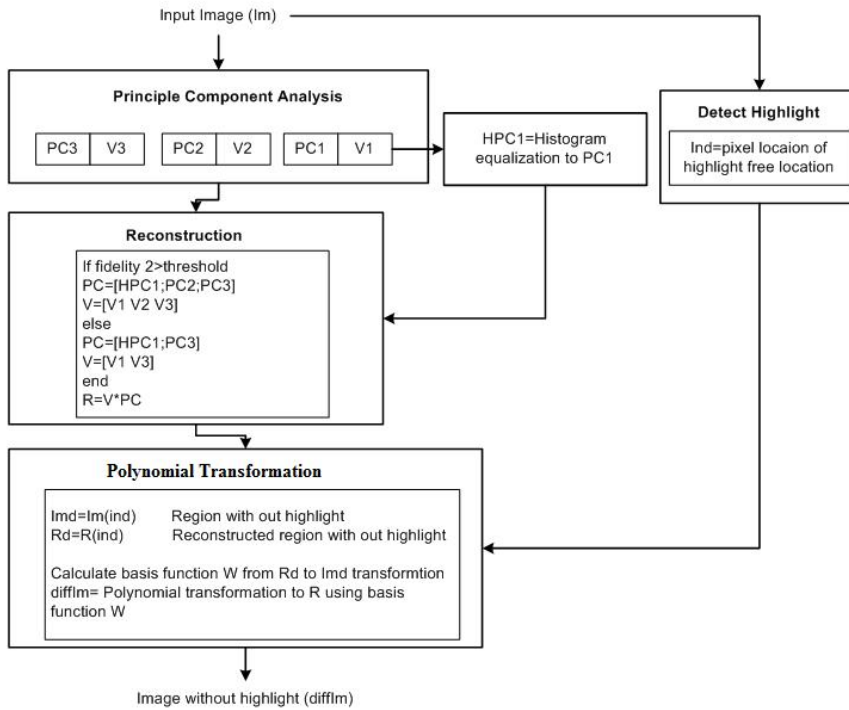


Figure 6.4: Highlight removal method applied in RGB image.

6.5 QUALITY MEASURE OF DIFFUSE IMAGE

There is in fact no exact ground truth diffuse image for the same illumination and viewing angles. Nevertheless, in the experiments on highlight removal from spectral images it has been assumed that the diffuse image obtained using a diffuse polarizer is the ground truth image. The diffuse image by polarizer can also be used as the ground truth image for the RGB image. But the ground truth object and test object should be measured at the same time under same conditions of measurement. The average S-CIELAB [78] difference image between the diffuse detected part of the test RGB image and the same part of diffuse image was used to analyze the quality of the results in *Publication 4*. Detailed implementation of S-CIELAB

has been presented in Appendix A.2.2. The less average error indicates a low color difference is obtained between the diffuse image and test image, and as a result the quality is better. The S-CIELAB color difference for some tested samples has been listed in Table 6.1.

Table 6.1: Average S-CIELAB color difference ΔE between the diffuse detected part of original image and final image after polynomial transformation. D is the standard deviation of S-CIELAB color difference. The original images and corresponding diffuse images are at Figure 6.3

	Pear	Face	Yellow ball	Green ball	Hat	Fish
ΔE	0.954	0.354	2.802	4.036	0.415	0.445
D	2.877	0.801	5.526	4.529	1.275	1.673

6.6 DISCUSSION

Highlight removal methods from RGB and spectral images have been proposed. In the proposed method for RGB image, histogram equalization was applied to first principal component of the images. In this experiment, second principal component was found carrying the large portion of informations of the highlight. However it can not be guaranteed for all the cases. So second principal component was included only if the fidelity ratio of second largest eigen vector is greater than threshold value otherwise rejected . The color of the reconstructed image gets shifted due to histogram equalization in first principal component. But reconstructed image is free of highlight. The color of the reconstructed image was corrected by using second order polynomial transformation. The weight vector of the polynomial transformation was obtained by using the transformation of the pixels of reconstructed image to the original image corresponding to highlight free pixels in original image. The accuracy of the result was evaluated by using S-CIELAB color difference formula in highlight free area. The diffuse image from diffuse polar-

izer can be used as the ground truth image for the the better quality evaluation. In another experiment for highlight removal from spectral image, calculated diffuse image was evaluated against the diffuse image by polarizer. The positive constrained spectral unmixing method has been proposed to remove the highlight from spectral image. At first, the highlight detection was done using K-means clustering in the one dimensional image produced by CEM and the endmembers of diffuse components were selected only from the diffuse part. The selected endmembers form diffuse part of image have been used to reconstruct diffuse image. The endmember of specular component should be selected at first, the best result will be achieved, if we know the SPD of used light source. Otherwise, the spectra as endmember of specular component that has the higher distance value can be used. The proposed method for spectral image has given promising result against the OSP method [33] and mixture model of probabilistic PCA method [67]. The comparisons between methods have been shown in Figure 6.5 and Figure 6.6. The proposed highlight removal method for spectral unmixing depends the quality of endmember of specular and diffuse component. Nevertheless, the diffuse image by spectral unmixing may also suffer from black spots in some parts of the image. A dark spot may occur in pixels that have spectra similar to the SPD of the light source because the spectrum that is similar to that of the light source has a fraction of diffuse component near to zero. The resultant spectra produced by this method always guarantee the positive spectra, which is not always the case in OSP method and probabilistic PCA method.

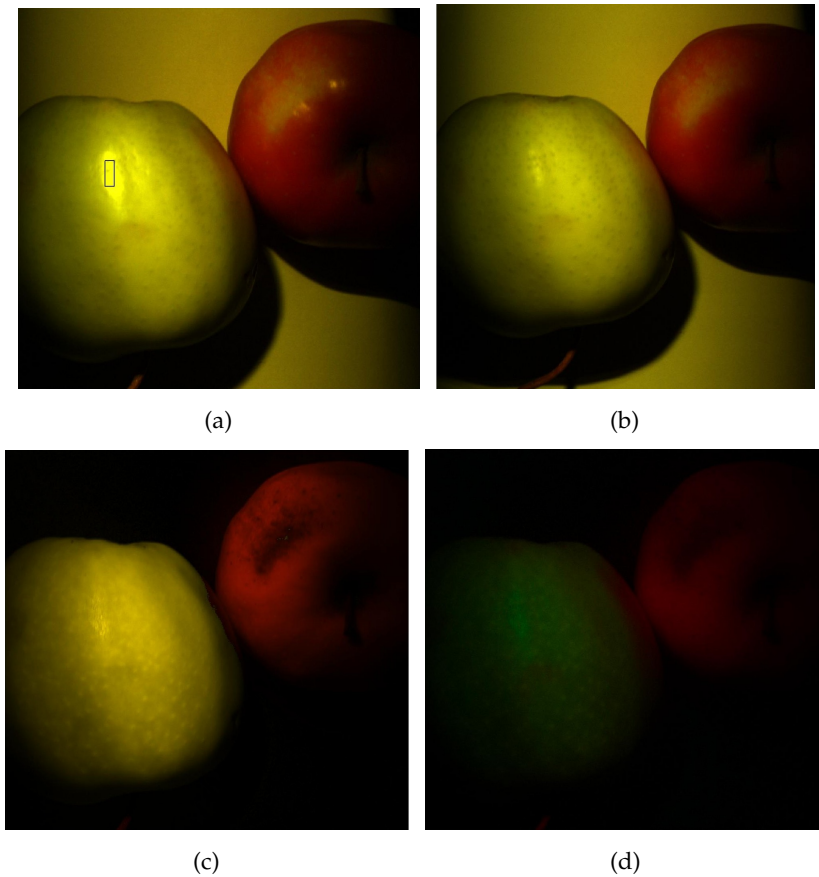


Figure 6.5: Constrained spectral unmixing method compared to polarizer method and OSP method: (a) Original spectral image (The radiance spectra of the selected part have been shown in Figure 6.6). (b) Highlight removed image by polarizer. (c) Highlight removed image by constrained spectral unmixing. (d) Highlight removed image by OSP method. All images are rendered in three bands [420 550 700] nm.

Highlight Removal from Single Image

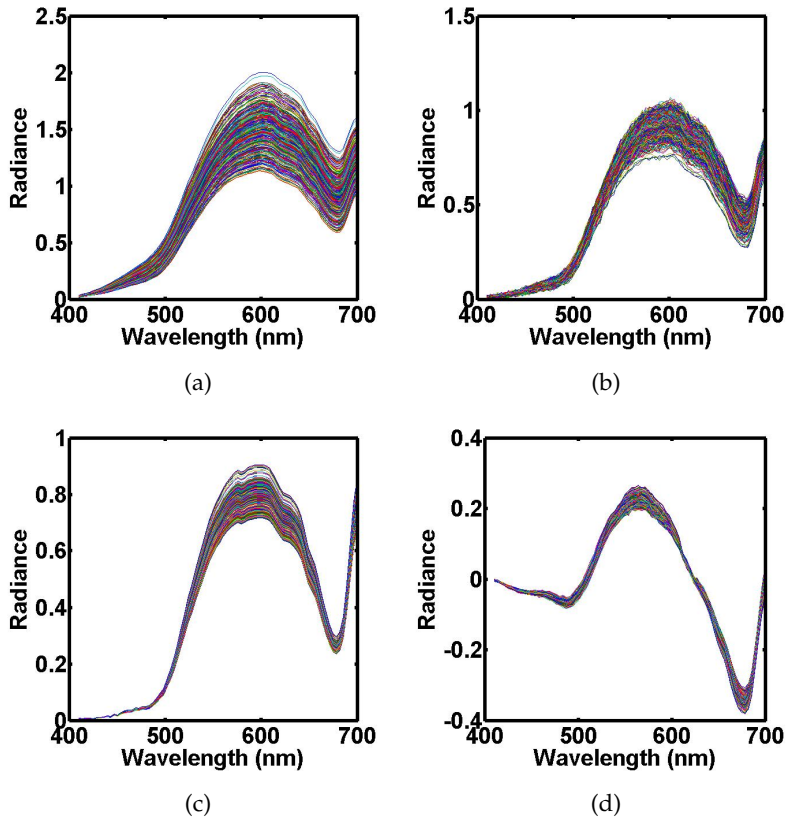


Figure 6.6: Comparison of radiance spectra obtained by polarizer, constrained spectral unmixing method and OSP method: (a) Radiance spectra from original image. (b) Radiance spectra from highlight removed image by polarizer. (c) Radiance spectra from highlight removed image by constrained spectral unmixing method. (d) Radiance spectra from highlight removed image by OSP. The radiance spectra are from the selected part of images shown in Figure 6.5.

7 Discussion

In recent years, due to technological developments in optics and detectors and the storage capacity in computers and computational power, the use of spectral imaging has increased in industrial applications and many research fields. Due to the high accuracy and voluminous information in a large number of bands, spectral imaging is becoming more popular in the measurement of the quality factors of objects.

In this thesis, spectral imaging has been exploited in analyzing a diffuse coated surface, highly glossy metallic and pearlescent coated surface and an image that suffers from highlight. The spectral image within the visible range of 380 *nm* to 780 *nm* has been used. For the pigment coated plastic surface the methods capable of finding the set of pigments to produce given pigments and predicting the required pigments from a set of given pigments have been proposed. The method employs the color spectra within the visible range, so it is called the spectral color mixing and unmixing method. The spectral color mixing and unmixing method have direct implications in industrial color management. The method reduces the expensive analytical base color mixing trial process. The metallic and pearlescent coated surface require reflectance measurement in different geometries for the accurate characterization of its reflectance, as their appearance depends on the measurement geometry. In this thesis a PCA and Wiener estimation-based method has been proposed to predict all the reflectances for all viewing angles just by using the reflectances measured in five angles. The method gives a feasible solution for industrial processes to determine the reflectances in desired viewing angles. Similarly, for the highlight affected surface, PCA and histogram equalization based method have been proposed to separate the diffuse and highlight component of the image. Positive constrained spectral unmixing method has been performed to separate diffuse and highlight com-

ponent in spectral image.

Publication 1 describes the spectral color mixing and unmixing method based on the KM method. Spectral color mixing produces the reflectance of a mixture from known reflectances of mixed pigments. In spectral unmixing the reflectances of the mixed pigments are predicted. In this technique the set of candidate unit k/s of the mixed pigments are selected from the set of unit k/s calculated from the training set provided. Concentrations of the mixed pigments are calculated using linear least square techniques. The method was tested on pigments coated on a plastic surface. The surface was considered an opaque surface. The method gives the set of mixed pigments sorted according to the spectral color difference calculated between given and predicted reflectance of the mixture. The main benefit of the method is the flexibility to the user to choose the set of mixed pigments according to quality requirements and price requirements. The method has direct implications in industrial processes. As future work, this method should be modified for transparent and semitransparent paints. A positive constrained linear least square technique can be tested instead of *LLS*.

The research on reflectance reconstruction and reflectance prediction in multi-angle measurement has been presented in *Publication 2* and *Publication 3*. The research provides the method to predict reflectance for a large number of viewing angles using the reflectance from a few viewing angles. Principal component analysis has been used to predict the reflectance in *Publication 2*. The methods were tested on metallic and pearlescent samples. *Publication 3* shows that the Wiener estimation method significantly improves the result if the polynomial order increases to the fifth order. In the method, the principal component vector should be calculated from the training set. The method can predict the reflectance for viewing angles which are outside the bounds of the given primary viewing angles but which are within the angles from where the reflectance of training sets were measured. The best viewing angles were selected using a full search among the angles that provide the local maxima and minima of the difference curve. The difference

curve was calculated as the root mean square error of the training set and its reconstruction. The required number of best viewing angles were determined according to the fidelity ratio calculated from the training set. In the future an optimal method, like orthogonal subspace projection, can be used to find the best primary angles.

Highlight removal method from the single image has been presented in *Publication 4* and *Publication 5*. In *Publication 4* a highlight removal method using histogram equalization and PCA in RGB image has been presented. The method was applied in the image without knowing the light source and detector type. The results look promising. In *Publication 5* a novel method in highlight removal from single spectral image using a positive constrained spectral unmixing method has been presented. The methods were compared against the existing method by orthogonal subspace projection by Fu *et al* [33] and principal component-based method by Bochko and Parkkinen [67]. Highlight removal from existing image is quite important to know the content of proper information. This method can be applied as a preprocessing step in the highlight-affected image, before applying further image processing. Real-time highlight detection and highlight removal from a single image will be the future direction. Real-time application has the great advantage of using as a preprocessing tool in real-time image analysis and image processing.

All the methods, performed in this thesis, have a direct implication in industrial applications. The method for spectral color mixing and unmixing was developed in collaboration with Exel. The developed application is in use in Exel to select the colorants. Similarly, the method of selection of best viewing angles and prediction of spectra in all viewing angles were developed as a part of industrial cooperation with Ruukki. Highlight removal method has the direct implication in the image processing and analysis. Highlight must be removed or reduced before the detection process, otherwise there is always chance of getting false result. The reflectance of mixed and mixture pigments, the reflectance of metallic and pearlescent coated samples in multi-angle measurement could be

successfully simulated and finally the spectra of a diffuse component from a highlight-affected image were simulated.

Bibliography

- [1] J. N. Mait, "A History of Imaging: Revisiting the Past to Chart the Future," *Optics & Photonics News* **17**, 22–27 (2006).
- [2] J. Parkkinen, T. Jääskeläinen, and M. Kuittinen, "Spectral representation of color images," in *9th International Conference on Pattern Recognition*, Vol. 2 (IEEE, 1988), pp. 933–935.
- [3] J. Parkkinen, "Spectral color imaging," in *13th Scandinavian Conference on Image Analysis (SCIA)*, Vol. 2749 (Springer, 2003), pp. 800–803.
- [4] G. Johnson and M. Fairchild, "Full-spectral color calculations in realistic image synthesis," *IEEE Computer Graphics and Applications* **19**, 47–53 (1999).
- [5] D. H. Foster, K. Amano, S. Nascimento, and M. J. Foster, "Frequency of metamerism in natural scenes," *Journal of Optical Society of America A* **23**, 2359–2372 (2006).
- [6] J. Lehtonen, J. Parkkinen, T. Jääskeläinen, and A. Kamshilin, "Principal component and sampling analysis of color spectra," *Optical review* **16**, 81–90 (2009).
- [7] J. Parkkinen, J. Hallikainen, and T. Jääskeläinen, "Characteristic spectra of Munsell colors," *JOSA A* **6**, 318–322 (1989).
- [8] M. Peercy, B. Zhu, and D. Baum, "Interactive full spectral rendering," in *Symposium on Interactive 3D graphics* (ACM Press, New York, 1995), pp. 67–68.
- [9] M. E. Schaepman, S. L. Ustin, A. J. Plaza, T. H. Painter, J. Verrelst, and S. Liang, "Earth system science related imaging spectroscopy-An assessment," *Remote Sensing of Environment* **113**, **Supplement 1**, S123–S137 (2009), Imaging Spectroscopy Special Issue.

- [10] R. Sandau, *Digital Airborne Camera: Introduction and Technology*, 1st ed. (Springer, Netherlands, 2010).
- [11] C. Fischer and I. Kakoulli, "Multispectral and hyperspectral imaging technologies in conservation: current research and potential applications," *Reviews in conservation* **7**, 3–16 (2006).
- [12] M. Hauta-Kasari, *Computational Techniques for Spectral Image Analysis*, Phd thesis (Lappeenranta University of Technology, 1999).
- [13] J. Schott, *Remote sensing: the image chain approach* (Oxford University Press, USA, 2007).
- [14] H. Liang, "Advances in multispectral and hyperspectral imaging for archaeology and art conservation," *Applied Physics A: Materials Science & Processing* 1–15 (2011).
- [15] M. Parker, "Emerging technology in cervical cancer screening: spectroscopy," *Clinical obstetrics and gynecology* **48**, 209–217 (2005).
- [16] K. Thorp and L. Tian, "A review on remote sensing of weeds in agriculture," *Precision Agriculture* **5**, 477–508 (2004).
- [17] A. Gowen, C. O'Donnell, P. Cullen, G. Downey, and J. Frias, "Hyperspectral imaging - an emerging process analytical tool for food quality and safety control," *Trends in Food Science & Technology* **18**, 590–598 (2007).
- [18] J. Setoain, M. Prieto, C. Tenllado, and F. Tirado, "GPU for parallel on-board hyperspectral image processing," *International Journal of High Performance Computing Applications* **22**, 424–437 (2008).
- [19] Y. Tarabalka, T. Haavardsholm, I. Kåsen, and T. Skauli, "Real-time anomaly detection in hyperspectral images using multivariate normal mixture models and GPU processing," *Journal of Real-Time Image Processing* **4**, 287–300 (2009).

Bibliography

- [20] A. Paz and A. Plaza, "GPU Implementation of Target and Anomaly Detection Algorithms for Remotely Sensed Hyperspectral Image Analysis," *Satellite Data Compression, Communication and Processing VI*, Proc. SPIE 7810, 1–10 (2010).
- [21] J. Molero, E. Garzón, I. García, and A. Plaza, "Anomaly detection based on a parallel kernel RX algorithm for multicore platforms," *Journal of Applied Remote Sensing* **6**, 1–10 (2012).
- [22] <http://www.avantes.com/news/avamouse.pdf> (Last viewed, 2007).
- [23] http://www.spectralcameras.com/files/downloads/VariSpec_Technote.pdf (Last viewed, 24.09.2010).
- [24] <http://www.hypex.no/products/hypex/vnir1600.php> (Last viewed, 03.07.2011).
- [25] P. Slater, "Radiometric considerations in remote sensing," *Proceedings of the IEEE* **73**, 997–1011 (1985).
- [26] J. Suomalainen, T. Hakala, J. Peltoniemi, and E. Puttonen, "Polarised multiangular reflectance measurements using the finnish geodetic institute field goniospectrometer," *Sensors* **9**, 3891–3907 (2009).
- [27] J. Palmer, "The measurement of transmission, absorption, emission, and reflection," *Handbook of optics* **2**, 251–255 (1995).
- [28] Y. Akao, R. Shogenji, N. Tsumura, M. Yamaguchi, and J. Tanida, "Efficient gonio-imaging of optically variable devices by compound-eye image-capturing system," *Optics Express* **19**, 3353–3362 (2011).
- [29] H.-C. Lee, "Method for computing the scene-illuminant chromaticity from specular highlights," *Journal of Optical Society of America A* **3**, 1694–1699 (1986).
- [30] S. A. Shafer, "Using color to separate reflection components," *Color Research & Application* **10**, 210–218 (1985).

- [31] A. Hanbury, "Physics-based Segmentation of Colour Images in Spherical Coordinates," (Technical Report PRIP-TR-84, PRIP, T.U. Wien, July 2003).
- [32] S. Tominaga, "Surface identification using the dichromatic reflection model," *IEEE Transactions on Pattern Analysis and Machine Intelligence* **13**, 658–670 (1991).
- [33] Z. Fu, R. T. Tan, and T. Caelli, "Specular Free Spectral Imaging Using Orthogonal Subspace Projection," in *Proceedings of the 18th International Conference on Pattern Recognition*, Vol. 1, ICPR '06 (2006), pp. 812–815.
- [34] R. H. Park and E. I. Stearns, "Spectrophotometric formulation," *Journal of Optical Society of America* **34**, 112–113 (1944).
- [35] G. Golub and W. Kahan, "Calculating the singular values and pseudo-inverse of a matrix," *Journal of the Society for Industrial and Applied Mathematics: Series B, Numerical Analysis* 205–224 (1965).
- [36] N. Keshava, "A survey of spectral unmixing algorithms," *Lincoln Laboratory Journal* **14**, 55–78 (2003).
- [37] Q. Du, I. Kopriva, and H. Szu, "Investigation on constrained matrix factorization for hyperspectral image analysis," in *Proceedings of Geoscience and Remote Sensing Symposium*, Vol. 6 (IEEE, 2005), pp. 4304–4306.
- [38] D. Lee and H. Seung, "Learning the parts of objects by non-negative matrix factorization," *Nature* **401**, 788–791 (1999).
- [39] P. Kubelka, "New Contributions to the Optics of Intensely Light-Scattering Materials. Part I," *Journal of Optical Society of America* **38**, 448–448 (1948).
- [40] H. R. Davidson and H. Hemmendinger, "Color Prediction Using the Two-Constant Turbid-Media Theory," *Journal of Optical Society of America* **56**, 1102–1109 (1966).

Bibliography

- [41] W. E. Vargas and G. A. Niklasson, "Applicability conditions of the Kubelka-Munk theory," *Applied Optics* **36**, 5580–5586 (1997).
- [42] J. L. Saunderson, "Calculation of the Color of Pigmented Plastics," *Journal of Optical Society of America* **32**, 727–729 (1942).
- [43] R. T. Marcus and P. E. Pierce, "An analysis of the first surface correction for the color matching of organic coatings from the viewpoint of radiative transfer theory," *Progress in Organic Coatings* **23**, 239–264 (1994).
- [44] L. Yang and B. Kruse, "Revised Kubelka–Munk theory. I. Theory and application," *Journal of Optical Society of America A* **21**, 1933–1941 (2004).
- [45] Y. Zhao and R. S. Berns, "Predicting the spectral reflectance factor of translucent paints using Kubelka-Munk turbid media theory: Review and evaluation," *Color Research & Application* **34**, 417–431 (2009).
- [46] H. G. Volz, *Industrial Color Testing: Fundamentals and Techniques* (Wiley-VCH, New York, 1995).
- [47] W. E. Vargas, "Inversion methods from Kubelka–Munk analysis," *Journal of Optics A: Pure and Applied Optics* **4**, 452 (2002).
- [48] E. Allen, "Colorant formulation and shading," *Optical radiation measurements* **2**, 289–336 (1980).
- [49] R. S. Berns and M. Mohammadi, "Single-constant simplification of Kubelka-Munk turbid-media theory for paint systems—A review," *Color Research & Application* **32**, 201–207 (2007).
- [50] C. S. Haase and G. W. Meyer, "Modeling pigmented materials for realistic image synthesis," *ACM Transactions on Graphics* **11**, 305–335 (1992).

- [51] N. Gossett and B. Chen, "Paint inspired color mixing and compositing for visualization," in *IEEE Symposium on Information Visualization* (IEEE, 2004), pp. 113–118.
- [52] R. Cook and K. Torrance, "A reflectance model for computer graphics," *ACM Transactions on Graphics* **1**, 7–24 (1982).
- [53] R. S. Berns, *Billmeyer and Saltzman's Principles of Color Technology*, 3rd ed. (John Wiley & Sons, New York, 2000).
- [54] P. Pierce and R. Marcus, "Radiative transfer theory solid color-matching calculations," *Color Research & Application* **22**, 72–87 (1997).
- [55] J. Nobbs, "Colour-match prediction for pigmented materials," *Colour physics for industry* 292–372 (1997).
- [56] A. Takagi, A. Watanabe, and G. Baba, "Prediction of spectral reflectance factor distribution of automotive paint finishes," *Color Research & Application* **30**, 275–282 (2005).
- [57] M. Nadal and E. Early, "Color measurements for pearlescent coatings," *Color Research & Application* **29**, 38–42 (2004).
- [58] L. Sung, M. Nadal, P. Stutzman, and M. McKnight, "Characterization of coating microstructure using laser scanning confocal microscopy," *Polymeric materials science and engineering* **83**, 343–344 (2000).
- [59] A. Rodrigues, "Measurement of metallic and pearlescent colors," *Die Farbe* **37**, 65–78 (1990).
- [60] A. Rodrigues, "Color technology and paint," in *Color and Paints Interim Meeting of the International Color Association Proceedings* (2004), pp. 103–108.
- [61] D. Alman, "Directional color measurement of metallic flake finishes," in *Proceedings of the ISCC Williamsburg Conference on Appearance* (1987), pp. 53–56.

Bibliography

- [62] H. Saris, R. Gottenbos, and H. Van Houwelingen, "Correlation between visual and instrumental colour differences of metallic paint films," *Color Research & Application* **15**, 200–205 (1990).
- [63] http://jp.hamamatsu.com/products/opto-meas/index_en.html (last viewed, 16.09.2012).
- [64] I. T. Jolliffe, *Principle Component Analysis*, Vol. 2 of *Series in Statistics*, 2nd ed. (Springer, 2002).
- [65] R. Baribeau, "Optimized spectral estimation methods for improved colorimetry with laser scanning systems," in *Proceedings of First International Symposium on 3D Data Processing Visualization and Transmission* (IEEE, 2002), pp. 400–404.
- [66] P. Stigell, K. Miyata, and M. Hauta-Kasari, "Wiener estimation method in estimating of spectral reflectance from RGB images," *Pattern Recognition and Image Analysis* **17**, 233–242 (2007).
- [67] V. Bochko and J. Parkkinen, "Highlight analysis using a mixture model of probabilistic PCA," in *WSEAS Transactions on Systems*, Vol. 4 (2005), pp. 55–59.
- [68] S. K. Nayar, X.-S. Fang, and T. Boult, "Separation of Reflection Components Using Color and Polarization," *International Journal of Computer Vision* **21**, 163–186 (1997).
- [69] G. J. Klinker, S. A. Shafer, and T. Kanade, "The measurement of highlights in color images," in *Color*, G. E. Healey, S. A. Shafer, and L. B. Wolff, eds. (Jones and Bartlett Publishers, Inc., USA, 1992), pp. 309–334.
- [70] R. T. Tan and K. Ikeuchi, "Separating Reflection Components of Textured Surfaces Using a Single Image," *IEEE Transactions on Pattern Analysis and Machine Intelligence* **27**, 178–193 (2005).
- [71] H.-L. Shen, H.-G. Zhang, S.-J. Shao, and J. H. Xin, "Chromaticity-based separation of reflection components in a single image," *Pattern Recognition* **41**, 2461–2469 (2008).

- [72] P. Tan, S. Lin, L. Quan, and H.-Y. Shum, "Highlight Removal by Illumination-Constrained Inpainting," in *Proceedings of the Ninth IEEE International Conference on Computer Vision, ICCV* (2003), pp. 164–169.
- [73] Q. Yang, S. Wang, and N. Ahuja, "Real-time specular highlight removal using bilateral filtering," *Computer Vision–ECCV 2010* 87–100 (2010).
- [74] C. Chang, "Orthogonal subspace projection (OSP) revisited: A comprehensive study and analysis," *IEEE Transactions on Geoscience and Remote Sensing* **43**, 502–518 (2005).
- [75] J. Harsanyi and C. Chang, "Hyperspectral image classification and dimensionality reduction: An orthogonal subspace projection approach," *IEEE Transactions on Geoscience and Remote Sensing* **32**, 779–785 (1994).
- [76] J. Hartigan and M. Wong, "Algorithm AS 136: A k-means clustering algorithm," *Journal of the Royal Statistical Society. Series C (Applied Statistics)* **28**, 100–108 (1979).
- [77] O. Frost III, "An algorithm for linearly constrained adaptive array processing," *Proceedings of the IEEE* **60**, 926–935 (1972).
- [78] X. Zhang, B. Wandell, et al., "A spatial extension of CIELAB for digital color image reproduction," in *SID International Symposium Digest of Technical Papers*, Vol. 27 (Society for information display, 1996), pp. 731–734.
- [79] D. Pascale, "A review of RGB color spaces," *The BabelColor Company, Montreal, Technical Report* (2003).
- [80] E. Giorgianni and T. Madden, *Digital color management: encoding solutions* (Addison-Wesley Longman, 1998).
- [81] L. Kheng, "Color Spaces and Color-Difference Equations," *Color Research and Application* **24**, 186–198 (2002).

Bibliography

- [82] G. Johnson and M. Fairchild, "A top down description of S-CIELAB and CIEDE2000," *Color Research & Application* **28**, 425–435 (2003).
- [83] M. Melgosa, "Testing CIELAB-based color-difference formulas," *Color Research & Application* **25**, 49–55 (2000).
- [84] R. McDonald, "European practices and philosophy in industrial colour-difference evaluation," *Color Research & Application* **15**, 249–260 (1990).
- [85] H. Mangine, K. Jakes, and C. Noel, "A preliminary comparison of CIE color differences to textile color acceptability using average observers," *Color Research & Application* **30**, 288–294 (2005).
- [86] K. Smith, "Colour-order systems, colour spaces, colour difference and colour scales," *Colour Physics for Industry. 2nd Ed. Bradford: Society of Dyers and Colourists* 121–130 (1997).
- [87] R. Yuhas, A. Goetz, and J. Boardman, "Discrimination among semi-arid landscape endmembers using the spectral angle mapper (SAM) algorithm," in *Summaries of the Third Annual JPL Airborne Geoscience Workshop*, Vol. 1 (Pasadena, CA: JPL Publication, 1992), pp. 147–149.

A Appendix: Supporting Equations

A.1 KUBELKA-MUNK METHOD FORMULATION

The Kubelka-Munk equation shown in Equation (4.3.1) is derived in this section. The pigmented solution is a paint applied with the uniform thickness X over a substrate of reflectance of R_g . Let I be the incident light which is transmitted down through the paint, either directly from the source or by the scattering of light from pigment particles. Let J be the light which is returning to the source, either by the reflection from the substrate or scattering of pigment particles. Consider a very thin sublayer of paint of thickness dx . The amount of light that is lost from I and J through the layer are shown in following equations.

$$(K + S) I dx \quad (\text{A.1.1})$$

$$(K + S) J dx \quad (\text{A.1.2})$$

Where K and S are the absorption and scattering coefficients respectively.

$$dI = (K + S)I dx - SJ dx \quad (\text{A.1.3})$$

$$- dJ = (K + S)J dx - SI dx \quad (\text{A.1.4})$$

As the light representing I and J travels in opposite directions, the change in their signs through the film are opposing. Equations (A.1.3) and (A.1.4) are written assuming $a = 1 + \frac{K}{S}$.

$$\frac{dI}{S dx} = aI - J \quad (\text{A.1.5})$$

$$-\frac{dJ}{S dx} = aJ - I \quad (\text{A.1.6})$$

Adding and rearranging Equations (A.1.5) and (A.1.6) lead to

$$\frac{I dJ - J dI}{I^2 S dx} = -2a \frac{J}{I} + \frac{J^2}{I^2} + 1 \quad (\text{A.1.7})$$

From the quotient rule

$$\frac{d(J/I)}{S dx} = -2a \frac{J}{I} + \frac{J^2}{I^2} + 1 \quad (\text{A.1.8})$$

Setting $r = J/I$ then it is

$$\frac{dr}{S dx} = r^2 - 2ar + 1 \quad (\text{A.1.9})$$

Taking integration leads to.

$$\int \frac{dr}{r^2 - 2ar + 1} = S \int dx \quad (\text{A.1.10})$$

When the thickness of the layer is zero, the reflectance is R_g by the substrate and at the thickness X the reflectance is R .

$$\begin{aligned} \int_{R_g}^R \frac{dr}{r^2 - 2ar + 1} &= \frac{1}{2b} \int_{R_g}^R \frac{dr}{r - (a+b)} - \frac{1}{2b} \int_{R_g}^R \frac{dr}{r - (a-b)} \\ &= \frac{1}{2b} \log \frac{(R - a - b)(R_g - a + b)}{(R - a + b)(R_g - a - b)} \end{aligned} \quad (\text{A.1.11})$$

Where $b = \sqrt{a^2 - 1}$, now Equation (A.1.10) is written as:

$$\frac{1}{2b} \log \frac{(R - a - b)(R_g - a + b)}{(R - a + b)(R_g - a - b)} = SX \quad (\text{A.1.12})$$

$$\frac{(R - a - b)(R_g - a + b)}{(R - a + b)(R_g - a - b)} = e^{2bSX} \quad (\text{A.1.13})$$

Now separating R from the other parts.

$$\begin{aligned} R &= \frac{1 - R_g \left(a - b \frac{e^{2bSX} + 1}{e^{2bSX} - 1} \right)}{a - R_g + b \frac{e^{2bSX} + 1}{e^{2bSX} - 1}} \\ &= \frac{1 - R_g (a - b \coth(bSX))}{a - R_g + b \coth(bSX)} \end{aligned} \quad (\text{A.1.14})$$

A.2 COLOR DIFFERENCE

The color difference formula is used to find the discrimination between two samples of colors. Here the CIELAB color difference, S-CIELAB color difference and CMC(l:c) color difference formulae have been presented. As a first step in the method, CIE tristimulus values should be calculated. In the second step, $L^*a^*b^*$ is calculated from the tristimulus values. Here L^* is the representation of luminance and a^* and b^* are the chrominance values. For the given illumination, sensitivity function and reflectance of the sample, the CIE tristimulus values are calculated as follows. For the given RGB, its CIE tristimulus is calculated by linear transformation according to the RGB type [79].

$$\begin{aligned}
 X &= K \int_{\lambda_{min}}^{\lambda_{max}} R_{\lambda} S_{\lambda} x_{\lambda} d\lambda \\
 Y &= K \int_{\lambda_{min}}^{\lambda_{max}} R_{\lambda} S_{\lambda} y_{\lambda} d\lambda \\
 Z &= K \int_{\lambda_{min}}^{\lambda_{max}} R_{\lambda} S_{\lambda} z_{\lambda} d\lambda
 \end{aligned} \tag{A.2.1}$$

Where X , Y and Z are CIE tristimulus values. R_{λ} is the reflectance of the reflective object. S_{λ} is the spectral density of the illuminating light. x_{λ} , y_{λ} and z_{λ} are the color matching functions of the CIE standard colorimetric observer. The multiplier K is chosen so that Y has the value 100 for a perfect white matt surface. A perfect white matt surface is an ideal non-fluorescent, isotropic diffuser with a reflectance equal to 1 ($R_{\lambda} = 1$) across the visible spectrum [53,80].

$$K = \frac{100}{\int_{\lambda_{min}}^{\lambda_{max}} S_{\lambda} y_{\lambda} d\lambda} \tag{A.2.2}$$

A.2.1 CIELAB color difference

The spacing of the colors in the XYZ space is not perceptually uniform [81]. The CIE X, Y, Z space can be converted to a more perceptually uniform CIE1976 $L^*a^*b^*$ (CIELAB) color space as follows.

$$\begin{aligned} L^* &= 116f\left(\frac{Y}{Y_w}\right) - 16 \\ a^* &= 500\left[f\left(\frac{X}{X_w}\right) - f\left(\frac{Y}{Y_w}\right)\right] \\ b^* &= 200\left[f\left(\frac{Y}{Y_w}\right) - f\left(\frac{Z}{Z_w}\right)\right] \end{aligned} \quad (\text{A.2.3})$$

Where,

$$\begin{aligned} f(t) &= t^{1/3} && \text{if } t > 0.008856 \\ f(t) &= 7.787t + \frac{16}{116} && \text{Otherwise} \end{aligned}$$

Here, X_w , Y_w and Z_w are the tristimulus values calculated from a perfect white matt surface ($R_\lambda = 1$ and $Y_w = 100$). The color difference formula for two color samples in CIELAB color space is as follows. The subscript indicates sample1 and sample2.

$$\Delta E_{lab} = \sqrt{(L_1^* - L_2^*)^2 + (a_1^* - a_2^*)^2 + (b_1^* - b_2^*)^2} \quad (\text{A.2.4})$$

A.2.2 S-CIELAB color difference

S-CIELAB is the extension of the CIELAB color metric applied to measure the color reproduction errors between images [78]. The notation ‘‘S’’ stands for spatial. The S-CIELAB difference measure reflects both spatial and color sensitivity, and it equals the color CIELAB over the uniform regions of the image [78]. The step by step implementation of the S-CIELAB calculation has been illustrated in Figure A.1. There is a linear transformation from a given RGB image to device independent CIE XYZ tristimulus values [79]. The device independent CIE XYZ value is transformed linearly to opponent color space AC_1C_2 as shown in Equation (A.2.5). Here,

A represents the achromatic representation that is luminance. Similarly, C_1 and C_2 are chromatic representations that are red-green and blue-yellow respectively.

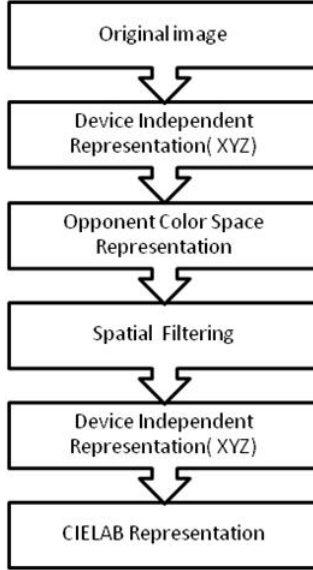


Figure A.1: Step by step calculation of S-CIELAB [78, 82].

$$\begin{bmatrix} A \\ C_1 \\ C_2 \end{bmatrix} = \begin{bmatrix} 0.279 & 0.72 & -0.107 \\ -0.449 & 0.29 & -0.077 \\ 0.086 & -0.59 & 0.501 \end{bmatrix} \begin{bmatrix} X \\ Y \\ Z \end{bmatrix} \quad (\text{A.2.5})$$

Spatial filtering is applied in each channel of the image represented by opponent color space. The two-dimensional spatial kernels used for filtering are shown in Equations (A.2.6) and (A.2.7) [78].

$$f = k \sum_i w_i E_i \quad (\text{A.2.6})$$

$$E_i = k_i e^{-(x^2+y^2)/\sigma_i^2} \quad (\text{A.2.7})$$

The parameter k_i is chosen so that E_i sums to 1 and the parameter k is chosen so that for each color plane, its two-dimensional kernel f sums to one [78]. As a result, it preserves the mean color values

for uniform areas [82]. The parameters w_i and σ_i represent the weight and spread (in degrees of visual angle) and the Gaussian functions respectively [82]. The filtered image is converted to device independent *CIE XYZ* tristimulus space. And finally *CIE XYZ* is converted to CIELAB, which is called S-CIELAB. The difference between the original image and the reproduced image calculated by Euclidean distance in S-CIELAB color space is called the S-CIELAB error.

A.2.3 CMC (l:c) color difference

CIELAB is a uniform color space, but different practical applications have shown better color differences by the setting of weighting factors [83,84]. CMC, CIE 94 and CIEDE 2000 each employ such weighting factors to adjust the inaccuracies [85]. In reference [85] it was found that CMC most closely represented the judgments of an average observer. The color difference formula ΔE proposed by the Society of Dyers and Colourists Color Measurement Committee *CMC(l : c)* as follows.

$$\Delta E_{CMC}(l : c) = \sqrt{\frac{(L_1^* - L_2^*)^2}{IS_L} + \frac{(C_{ab,1}^* - C_{ab,2}^*)^2}{CS_c} + \frac{(h_{ab,1} + h_{ab,2})^2}{S_h}} \quad (A.2.8)$$

In Equation (A.2.8), the subscripts 1 and 2 are the notation for the samples to be compared. L^* is the luminance as in CIELAB and C_{ab}^* and h_{ab} is the notation of the chroma and hue of the samples. Chroma and hue is calculated from CIELAB chrominance a^* and b^* . Chroma and hue is the radial and angular component in coordinates representing the X and Y axes by a^* and b^* respectively as shown in Figure A.2.

$$C_{ab}^* = \sqrt{a^{*2} + b^{*2}} \quad (A.2.9)$$

$$h_{ab} = \tan^{-1} \left(\frac{b^*}{a^*} \right) \quad (A.2.10)$$

Appendix: Supporting Equations

Here,

$$\begin{aligned}
 0^\circ < h_{ab} < 90^\circ & \quad \text{if } a^*, b^* > 0 \\
 90^\circ < h_{ab} < 180^\circ & \quad \text{if } a^* < 0, b^* > 0 \\
 180^\circ < h_{ab} < 270^\circ & \quad \text{if } a^*, b^* < 0 \\
 270^\circ < h_{ab} < 360^\circ & \quad \text{if } a^* > 0, b^* < 0
 \end{aligned}$$

In Equation (A.2.8), S_L , S_c and S_h are the relative attributes difference for the luminance, chroma and hue calculated from the standard observer [86].

$$S_L = \frac{0.040975 L^*}{1 + 0.01765 L^*} \quad \text{for } L^* > 16$$

$$S_L = 0.511 \quad \text{for } L^* < 16$$

$$S_c = \frac{0.0638 c^*}{1 + 0.0131 c^*} + 0.0638$$

$$S_h = (F T + 1 - F) S_c$$

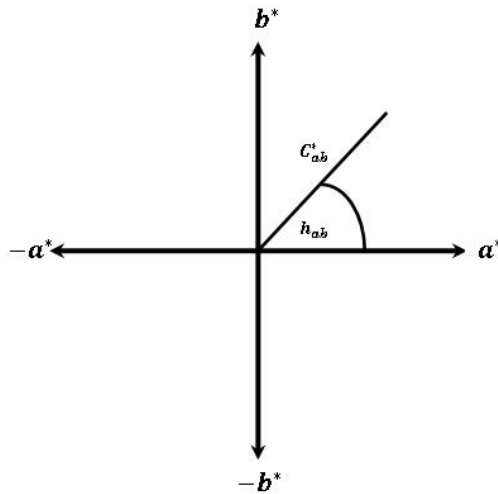


Figure A.2: Chroma and hue representation in CIELAB.

Where,

$$F = \sqrt{\frac{c^{*4}}{c^{*4} + 1900}}$$

$$T = 0.36 + |0.4 \cos(35 + h)| \quad \text{for } h = 164^\circ \text{ or } h > 345^\circ$$

$$T = 0.56 + |0.2 \cos(168 + h)| \quad \text{for } 164^\circ < h < 345^\circ$$

A.3 SPECTRAL DIFFERENCE

Spectral difference between two spectra , like radiance or reflectance should be calculated by considering all wavelengths.

A.3.1 Root Mean Square Error

Root mean square error (*RMSE*) between two spectra R_1 and R_2 is euclidean distance between two spectra divided by square root of total number of bands.

$$RMSE = \sqrt{\frac{\sum_{i=1}^n (R_1(i) - R_2(i))^2}{n}} \quad (\text{A.3.1})$$

In Equation (A.3.1), i represents the index of wavelengths and varies from 1 to n , since n is the number of wavelengths.

A.3.2 Spectral angle mapper

Spectral angle mapper calculates the angular distance between spectra [87]. It measures the similarity between two spectra looking the shape of the objects rather than its magnitude. The cosine value of the angle is also called the GFC (goodness of fit coefficient).

$$\cos(\theta) = \frac{\sum_{i=1}^n R_1(i)R_2(i)}{\sqrt{\sum_{i=1}^n R_1(i)^2} \sqrt{\sum_{i=1}^n R_2(i)^2}} \quad (\text{A.3.2})$$

Appendix: Supporting Equations

In Equation (A.3.2), $\cos(\theta)$ is the *cosine* of the angular distance θ between two spectra. $R_1(i)$ and $R_2(i)$ are the spectra value at i , here i is index of wavelength. The value of i varies 1 to n , when total number of wavelengths is n .

PESAL KOIRALA
*Simulation and
Measurement of Colored
Surfaces*

The objective of this thesis is to investigate the reflectance prediction of colored surfaces. Reflectance prediction methods in three different cases were proposed. In the first case, spectra of mixed pigments were simulated as well as spectra of mixing pigments and their concentrations were predicted. In the second case, spectra in multi-angle measurement were predicted. In order to predict correct reflectance in different viewing angles, the best viewing angles were determined. The proposed method was applied in metallic and pearlescent samples. In the third case, highlight removal method for RGB and spectral images were proposed.



UNIVERSITY OF
EASTERN FINLAND

PUBLICATIONS OF THE UNIVERSITY OF EASTERN FINLAND
Dissertations in Forestry and Natural Sciences

ISBN: 978-952-61-1078-3 (Printed)

ISSNL: 1798-5668

ISSN: 1798-5668

ISBN: 978-952-61-1079-0 (PDF)

ISSN: 1798-5676 (PDF)